Hydrodynamic dispersion within porous biofilms

Y. Davit,[1,2,3] H. Byrne,[1,4] J. Osborne,[4] J. Pitt-Francis,[4] D. Gavaghan,[4] and M. Quintard[2,3]
[1]*Mathematical Institute, University of Oxford, 24-29 St Giles', Oxford OX1 3LB, United Kingdom*
[2]*Université de Toulouse; INPT, UPS; Institut de Mécanique des Fluides de Toulouse (IMFT), Allée Camille Soula, F-31400 Toulouse, France*
[3]*CNRS IMFT, F-31400 Toulouse, France*
[4]*Department of Computer Science, Oxford University, Wolfson Building, Parks Road, Oxford OX1 3QD, United Kingdom*

Many microorganisms live within surface-associated consortia, termed biofilms, that can form intricate porous structures interspersed with a network of fluid channels. In such systems, transport phenomena, including flow and advection, regulate various aspects of cell behavior by controlling nutrient supply, evacuation of waste products, and permeation of antimicrobial agents. This study presents multiscale analysis of solute transport in these porous biofilms. We start our analysis with a channel-scale description of mass transport and use the method of volume averaging to derive a set of homogenized equations at the biofilm-scale in the case where the width of the channels is significantly smaller than the thickness of the biofilm. We show that solute transport may be described via two coupled partial differential equations or telegrapher's equations for the averaged concentrations. These models are particularly relevant for chemicals, such as some antimicrobial agents, that penetrate cell clusters very slowly. In most cases, especially for nutrients, solute penetration is faster, and transport can be described via an advection-dispersion equation. In this simpler case, the effective diffusion is characterized by a second-order tensor whose components depend on (1) the topology of the channels' network; (2) the solute's diffusion coefficients in the fluid and the cell clusters; (3) hydrodynamic dispersion effects; and (4) an additional dispersion term intrinsic to the two-phase configuration. Although solute transport in biofilms is commonly thought to be diffusion dominated, this analysis shows that hydrodynamic dispersion effects may significantly contribute to transport.

I. INTRODUCTION

Biofilms are sessile communities of microbes that develop on solid or liquid interfaces, embedded within extracellular polymeric substances (EPS) [1]. These aggregations of microorganisms represent the dominant form of microbial life on Earth and have considerable sanitary, ecological, and economic impact. Effects can be desirable (wastewater processes, bioremediation, industrial and drinking water treatment, sequestration of carbon dioxide) or undesirable (paper manufacture, microbially influenced corrosion within pipelines, heat exchangers, or on ships) and, potentially, harmful (contamination in the food industry, disease, chronic infections, sustainability of water supply networks). Within the last few decades, understanding and controlling biofilm growth have emerged as major scientific challenges. An important component of these challenges is to understand how chemicals and particles are transported within biofilms, in order to (1) elucidate their resistance to antimicrobial agents; (2) design efficient control and staining strategies; (3) develop reliable growth models; and (4) describe the exchange of signaling molecules or genetic material between cells. These transport phenomena generally result from coupled biological, physical, and chemical processes occurring over a large spectrum of temporal and spatial scales.

In the early days of biofilm research, mathematical and conceptual models treated these consortia of microorganisms as a homogeneous coating of a solid surface. Later on, experiments showed that biofilms can form intricate architectures with pores, voids, and channels. For example, Stoodley *et al.* [2] used confocal laser scanning microscopy (CLSM) to perform particle image velocimetry (PIV) analysis and map the velocity field within biofilms grown under different conditions. They reported fluid flow inside biofilm channels and observed situations in which water flowed against the main current of the bulk water phase. Massol-Deyá *et al.* [3] used CLSM and scanning electron microscopy to observe multispecies aerobic biofilms growing in a granular activated-carbon fluidized-bed reactor. They describe channel-like and coral-reef structures. Hidalgo *et al.* [4] used CLSM to obtain tomographic *p*H images of highly heterogeneous biofilms. Advances in optical coherence tomography (OCT) also suggest complicated geometries. Wagner *et al.* [5] analyzed the structure of heterotrophic biofilms on relatively large volumes using OCT and revealed an incredible level of complexity.

Wimpenny *et al.* [6,7] and Loosdrecht *et al.* [8] suggest that these heterogeneities may result from a combination of factors including shear stress, diffusion limitations, and substrate concentration. Davey *et al.* [9] showed that the architecture of *Pseudomonas aeruginosa* biofilms is actively regulated by the production of rhamnolipid surfactants. Houry *et al.* [10] show that planktonic bacteria propelled by flagella can create large transient pores in the cell cluster and suggest that swimmers "may improve biofilm bacterial fitness by increasing nutrient flow in the matrix." It has also emerged—for example, see discussions by Plalkovà *et al.* [11]—that wild strains in real environments tend to form more heterogeneous structures than laboratory strains. These results have led to the idea that biofilms are complex structures, rather than dense impermeable gel-like layers. These studies have also identified two classes of channels, as discussed in Ref. [6] and illustrated

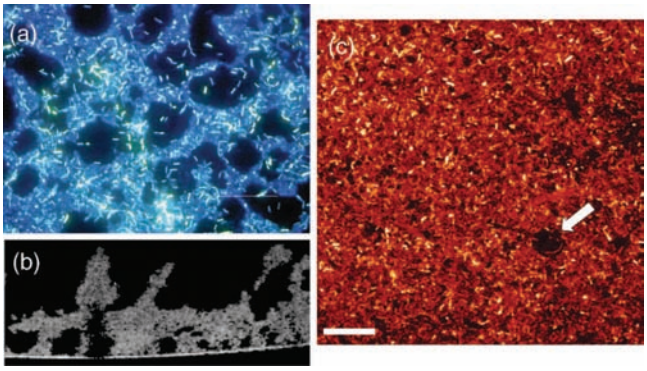

FIG. 1. (Color online) Examples of heterogeneous biofilms and fluid channels. (a) Top view of a polymicrobic biofilm grown on stainless steel where water channels have formed between the cell clusters (public domain, reproduced from Ref. [13]). (b) Cross-sectional view of intracluster channels obtained using optical coherence tomography (reproduced, with permission, from Ref. [5]). (c) Top view of a *Bacillus thuringiensis* biofilm where the arrow indicates a transient channel created by swimmers (reproduced from Ref. [10]).

in Fig. 1 (see also images in Ref. [4] and [12]): intracluster channels that may result from mechanical interactions with the fluid phase, fracturing of cell clusters, predation, or swimmers; and extra-cluster channels that form between cell clusters. We remark that most studies have focused on biofilms grown on flat surfaces and that the intra- versus extra-cluster distinction may be inappropriate for biofilms grown on more intricate substrata. *In the remainder of this work, we will use the generic terminology "channel" to specify passages (over a range of sizes and from different origins) through which fluids may flow and "porous biofilms" to describe heterogeneous biofilms involving channels, voids, or pores.*

The realization that biofilms can form intricate porous systems has led to the emergence of models which include fluid flow. For example, Dupin *et al.* [14] and Thullner and Baveye [15] determined the velocity field within the bulk fluid phase, viscosity μ_f, and within the biofilm by considering a fictitious weighted viscosity within the biofilm phase, $\mu_b = \gamma\mu_f$ with $\gamma \geqslant 1$. Kapellos *et al.* [16] developed a simulator that couples a cellular automaton with multiscale methods. They used a single-domain volume-averaged formulation, originally developed for Darcy-scale fluid-porous interfaces (see in Ref. [17]), to model the fluid flow within the bulk fluid and biofilm phases. Surprisingly, these studies have focused on momentum transport, and have not addressed the effects of biofilm permeability on mass transport. Within these structures, transfer of a molecule, or a particle, is influenced by a number of mechanisms, including advection, which may significantly impact the transport properties of important chemical species, such as nutrients or antimicrobial agents. Models should carefully incorporate these mechanisms into the mathematical description of biofilms.

Solute transport in biofilms, regardless of their architecture, is often characterized by the ratio D_e/D_{aq}, of the effective diffusion coefficient D_e and reference (culture medium or growth fluid) diffusion coefficient D_{aq}. Various experimental techniques have been used to calculate the effective diffusion coefficient; a review of these techniques can be found in Ref. [18] and further discussions are available in Refs. [19,20]. For the purposes of this paper, we outline the main experimental devices that have been used to measure effective diffusion coefficients, including recent developments. Bungay *et al.* [21] used the oxygen microelectrode technique, while Matson and Characklis [22] used a two-chamber method to measure oxygen and glucose diffusion coefficients in sludge flocs. de Beer *et al.* [23] used a combination of oxygen microelectrode measurements and CLSM to correlate concentration gradients with the structure of aerobic biofilms. Lawrence *et al.* [24] observed the diffusion of fluorescein and fluor-conjugated dextran in *Pseudomonas fluorescens* using fluorescence recovery after photobleaching (FRAP) and CLSM. Bishop *et al.* [25] calculated the effective diffusion coefficient from the structure of frozen 10–20-μm slices of biofilm. Stewart *et al.* [26] measured the diffusion coefficient of tagged daptomycin in cells clusters of *Staphylococcus epidermis* using CLSM. Recently, methods involving nuclear magnetic resonance (NMR) were proposed to obtain effective diffusion coefficients *in situ* [27,28]. Advances in x-ray microtomography also offer new perspectives for studying *in situ* transport properties in porous structures [29,30] and for estimating the corresponding diffusion coefficients.

Although D_{aq} is well defined for a given temperature, solute, and growth medium, the interpretation of D_e is ambiguous. Active biological processes, such as uptake rates, or physicochemical properties of the biofilm, the solute, and the bulk fluid phase, are difficult to correlate with D_e. Many studies have focused on identifying those parameters that most strongly influence D_e. Several authors have proposed empirical relationships between D_e/D_{aq} and the biofilm density ρ for passive transport [31]. Hinson and Kocher [32] used the fraction of EPS as an additional parameter. Stewart [18] investigated the influence of chemical properties on D_e/D_{aq}, such as the charge of the EPS or the molecular weight of the solute molecules. These correlations could be extended in many ways to account for other biochemical processes. Such formulas are extremely important because they can be widely used by experimentalists. However, many fundamental aspects of solute transport are still a matter of debate [33]. For example, the following points have received little attention from a mathematical modeling point of view. Biofilms are known to form heterogeneous structures (see [34]), with spatially and dynamically varying diffusion coefficients. This raises several fundamental questions, such as: How does such heterogeneity influence D_e? Is it valid to use a single effective value of the diffusion coefficient, or should a spatially resolved coefficient be used? With regard to advection within biofilms, is it possible to characterize solute transport in terms of the ratio D_e/D_{aq} when there is fluid flowing within the biofilm? Is it even possible to define effective diffusion coefficients in this case? With regard to reaction, do uptake rates and degradation of the solute influence the ratio D_e/D_{aq} or do they only affect the effective reaction rate?

In addition to the above theoretical issues, there is often ambiguity in the interpretation of experimental estimates for D_e. Recently, Wagner *et al.* [5] emphasized this problem by comparing estimates of biofilm porosities obtained using OCT and CLSM. For a Reynolds number of 4000 in the bulk fluid

phase, the porosity of the biofilm was found to be about 0.98 using CLSM and 0.35 using OCT. The authors suggest that OCT provides a more reliable framework for studying biofilm structures because it does not require fluorescence staining, and therefore does not rely on the transport properties of the biofilm, and is not limited by laser penetration depth. This is an important observation because CLSM is widely used to measure structural biofilm properties, and this may lead to erroneous conclusions. These results have wider implications that go beyond the issue of CLSM applicability: they suggest that caution should be exercised when interpreting experimental data for biofilms.

All the techniques discussed above differ in terms of their physical significance, and parameters, such as D_e, should be defined in relation to a specific experiment. Particularly relevant to this discussion is the spatial resolution of the experimental method under consideration. For example, the NMR technique used in Ref. [28] has an in-plane resolution of 7.5×250 μm, whereas x-ray microtomography and/or OCT can resolve to several micrometers. CLSM can achieve a similar resolution, but this is strongly dependent on the fluorescent staining. Two-chamber experiments only capture bulk information within each chamber. The parameters that are measured using these techniques are averaged over different volumes, and their physical interpretation is different. For example, if the biofilm contains fluid channels of approximate width 10 μm, then a technique with a resolution of 100 μm is measuring a concentration field and/or a diffusion coefficient averaged over both the cell clusters and the channels. On the other hand, a technique with a resolution of several micrometers can delineate between the two and/or provide a local diffusion coefficient for layered cell clusters. Experimental studies should carefully address these issues.

Upscaling techniques, such as volume averaging with closure (see [35]), can be used rigorously to define the ratio D_e/D_{aq} and, therefore, to address the above theoretical and experimental issues. With such techniques, averaged equations at the biofilm scale can be obtained from transport equations at the channel and cellular scales, *provided that several spatial and temporal scale constraints are satisfied*. An important feature of this approach is that the set of homogenized partial differential equations contains effective coefficients that can be directly related to the topology of the problem at the microscale, thereby allowing physical understanding of the contribution of the different processes. In addition, these methods may be used to develop novel ways of measuring effective diffusion coefficients. In particular, real geometries and velocity fields obtained via imaging techniques, e.g., tomography, may be directly used for the computation of effective coefficients. This strategy is an alternative to the standard inverse optimization method where effective coefficients are determined by optimization of model parameters using biofilm-scale data. A clear advantage of the upscaling method when compared with inverse optimization is that the effective parameters and the scale constraints are unambiguously defined. A disadvantage of this approach is that the experimental techniques that capture the information necessary for such calculations are new and the complete imaging-upscaling strategy has not yet been fully applied to real systems.

Even so, there is another advantage to homogenization techniques that does not require accurate knowledge of real geometries: *it yields the domains of validity of the models*. The mathematical procedure of homogenization generally involves order of magnitude estimates which apply to dimensionless numbers. For instance, in the case of Taylor dispersion, one usually requires that the Péclet number is such that the time for a molecule to diffuse radially is much smaller than the time for longitudinal transport. In addition, the averaging procedure, as presented in this paper, applies to an ensemble of geometries that is defined by length scale constraints. Therefore, models are not limited to a given geometry, but to a class of geometries, and the domains of validity apply to this entire class. Similarly, dimensionless numbers can be used to study important features of the models on simplified systems. For example, we can readily answer one of the questions presented above: Do uptake rates and degradation of the solute influence the ratio D_e/D_{aq} or do they only affect the effective reaction rate? In Refs. [36] and [37], it is shown using two-dimensional unit cells that the longitudinal dispersion coefficient decreases with the Damköhler number, $\mathcal{D}a$, or equivalently the Thiele modulus, when $\mathcal{D}a \gtrsim 10$. The quantitative behavior will change with the geometry but not the order of magnitude estimate. This is important because it means that for, say, $\mathcal{D}a \leqslant 1$, we can consider that the effective diffusion is the same for the reactive and nonreactive cases. Unfortunately, there is little experimental data that can be used to estimate $\mathcal{D}a$, essentially because its estimation requires knowledge of the diffusion coefficient, the form of the reaction rate, and the values of the reaction parameters. Stewart and Raquepas [38] calculated the Thiele modulus for reactive antimicrobial agents and found values in the range 0.44–18.2, suggesting that both situations may be encountered.

In this work, we will focus on the nonreactive case and use the volume averaging method to study some physical aspects of solute dispersion within porous biofilms. As discussed above, the analysis also applies to the reactive case when the dispersion coefficients do not depend upon uptake rates, i.e., when $\mathcal{D}a \leqslant 1$. Similar developments were presented in Refs. [35,39,40], but these papers focused on upscaling solute transport *from the cellular to the cell cluster scale*. The effect of advection within channels was studied in Ref. [40] but only in the limiting case where spatial gradients at the microscale are negligible, a situation termed local mass equilibrium. Here, we do not assume local mass equilibrium and show that relaxing this assumption leads to significant changes to the macroscale equations. Our modeling framework requires that biofilms should not be defined as cell clusters alone, but as a two-phase mixture of a cell cluster phase (ω) interspersed with a fluid-flow-channel phase (κ). We use a multiscale strategy to derive an effective diffusion tensor for this situation. Within the cell-EPS matrix (i.e., the cell clusters) the solute is transported by diffusion alone, but the diffusion coefficient can vary "arbitrarily" (although smoothly) in space. In the channels, the solute is transported by advection and diffusion.

Our primary goal is to answer the following questions:

(1) Are hydrodynamic dispersion effects significant within porous biofilms?

(2) Can we define an effective diffusion which describes fluid flow within the channels and spatially varying diffusion

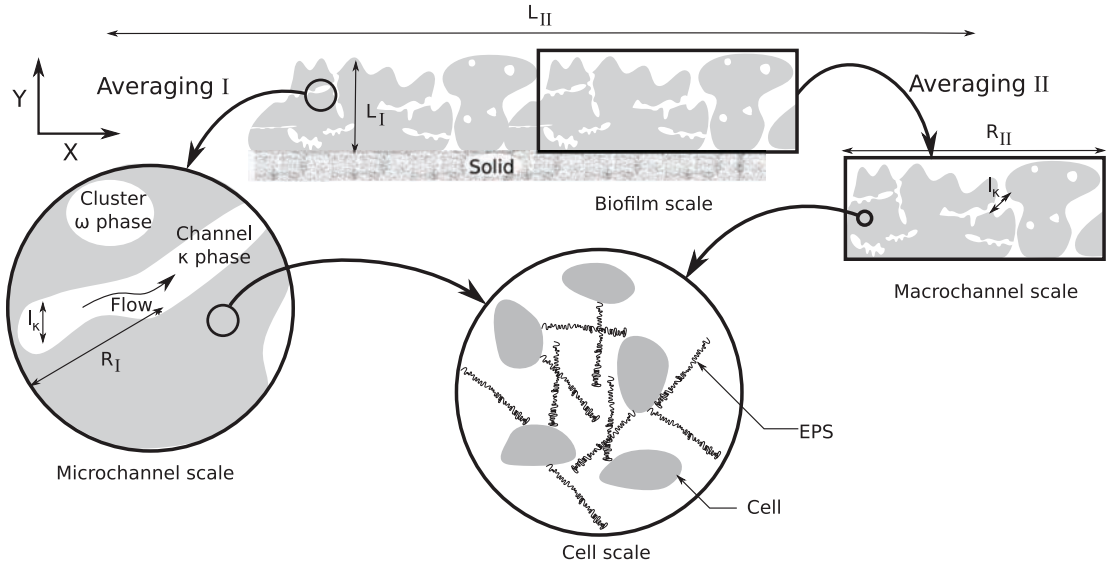

FIG. 2. Schematic diagram highlighting the multiscale nature of biofilms. Two different ways of averaging are presented depending on the scale constraints that are satisfied: on the left, the averaging volume is defined on a small portion of the biofilm; this is appropriate if the average diffusion coefficient within the cell clusters varies slowly throughout the biofilm and if channels are relatively small (i.e., $R_{\rm I} \ll L_{\rm I}$); on the right, the averaging volume is defined over the entire height of the biofilm, with a diffusion coefficient within the cell clusters which varies with depth and macrochannels (i.e., only $R_{\rm II} \ll L_{\rm II}$). Three spatial scales can be identified: the biofilm scale, the channel scale, and the cell scale. Each region illustrates a representative elementary volume of the corresponding larger scale. We remark that, for averaging II, the macroscale concentration fields within the biofilm will only vary along the X direction and boundary conditions should be treated carefully. In this work, we will focus primarily on upscaling from the channel scale to the biofilm scale with averaging I and defer averaging II to future work.

coefficients within the cell clusters? What are the physical processes corresponding to these effective dispersion coefficients?

(3) Should we always use the effective diffusion model to describe solute transport within porous biofilms? What are the alternatives?

The remainder of this study is organized as follows. In Sec. II, we briefly review experimental evidence for hydrodynamic dispersion within porous biofilms. In Sec. III, we detail our microscale problem. A representative elementary volume (REV) of the system is presented in Fig. 2 and the corresponding mathematical model at the channel scale is presented in Sec. III. We are interested in hierarchical systems for which $l_\kappa \ll R \ll L$, where l_κ is a characteristic width of the channels, R is the radius of the REV, and L is a characteristic macroscale length for the biofilm. In Sec. IV, we perform a perturbation analysis, termed the volume averaging with closure technique, to derive the macroscale models. For brevity, the key results are presented in the main text, while technical details are provided in the Appendix or in specific references. In Sec. VII, we discuss potential applications of these models, their limitations, and future work. In Sec. VIII, we summarize the main modeling results and the answers to the above questions.

II. EXPERIMENTAL EVIDENCE OF HYDRODYNAMIC DISPERSION EFFECTS IN BIOFILMS

It is now commonly accepted that channels are an essential part of biofilms (see [20]) and that advection effects are integral to solute transport within such systems. Even so, the channels and cell clusters are traditionally treated as two distinct phases. In Ref. [19], when discussing the issue of diffusion limitation inside cell clusters, Stewart states that "structural heterogeneity in a biofilm changes the geometry of the diffusion problem, but it does not alter the fundamental phenomena." Our goal in this section is to challenge this view. We argue that, while the microscale balance equations rely on advective and diffusive transport models, the fundamental phenomena captured by the notion of effective diffusion depend *on both the scale of observation and the structural heterogeneities*. Indeed, the homogenization of a problem with diffusion and advection at the microscale will produce a continuum representation in which the phase delineation has disappeared but in which the effective parameters depend on the heterogeneities. For example, effective dispersive fluxes will contain hydrodynamic dispersion effects that originate from fluctuations in the velocity field and tortuosity effects that describe the geometry of the microstructure. Similarly, within porous biofilms, we anticipate that there will be hydrodynamic dispersion effects produced by fluctuations in the velocity fields and tortuosity effects that will reflect the topology of the channel network within the biofilm. In this section, we provide experimental evidence that hydrodynamic dispersion may indeed occur. Our demonstration is based on the following two classes of experiments: (1) biofilm-scale measurements of effective diffusion that have reported $D_e/D_{\rm aq} > 1$; and (2) channel-scale measurements of the velocity field within a biofilm which suggest that advection effects may be important.

We start with biofilm-scale measurements and focus on studies that have reported peculiarities in the ratio $D_e/D_{\rm aq}$. In most cases, the ratio $D_e/D_{\rm aq}$ ranges between 0.1 and 1 (e.g., in

TABLE I. Examples of studies in which the effects of dispersion and advection have been observed in biofilms and biopellets.

Object	Chemicals	Technique	Diffusion ratio	Reference
Biofilm	$NaNO_3$ NaCl Oxygen	Two-chamber μ electrodes	$0.1 < D_e/D_{aq} < 1.1$	Horn and Morgenroth [41]
Biopellets	Oxygen	μ electrodes	$0.2 < D_e/D_{aq} < 1.5$	Hille *et al.* [42]
Biofilm/agar	Gd-DTPA	MRI	$D_e/D_{agar} = 1.44$	Ramanan *et al.* [43]
Biofilms	Review	Review	$0.11 < D_e/D_{aq} < 2$	Melo [33]

Ref. [19]). In these situations, the path of a solute molecule in a cell cluster is constrained by the presence of obstacles (cells, extracellular polymeric substances, abiotic particles) and a notion of tortuosity can be invoked [33]. Interestingly, in some low-density biofilms and in fungal biopellets, this ratio has also been reported to be larger than unity (cf. Table I). Melo [33] argues that the tortuosity, Λ, defined by $D_e = D_{aq}/\Lambda$, can be lower than unity if the solute undergoes convection inside the biofilm. This is an interesting idea, but it also suggests that a lot of physics is hidden within D_e and that a notion of tortuosity alone might not be sufficient. Hydrodynamic dispersion can be used to interpret these results if the Péclet number, $\mathrm{Pe} = \frac{\upsilon d}{D_{aq}}$, where υ is an average velocity and d a characteristic length, is sufficiently large. In the case of the biopellets, the flow is not limited by the EPS, and even larger ratios, $D_e/D_{aq} > 1$, have been reported when the cell density is relatively low (e.g., in Ref. [42], Fig. 3, p. 1207).

Even when $D_e/D_{aq} < 1$, it is not straightforward to determine the relative contributions of diffusion and advection to solute transport. It is commonly accepted that $D_e/D_{aq} < 1$ corresponds to a diffusion-dominated transport. For instance, Horn and Morgenroth [41] clearly state that "[...] convective transport would have resulted in $D_e/D_{aq} > 1$. The results presented indicate that for biofilms older than a few days and with mean biofilm density higher than 20 kg/m^3 convective transport can be neglected." We question this interpretation. In the case of porous biofilms, $D_e/D_{aq} < 1$ means that the combined effects of the advective and diffusive "components" (a clear definition of these components is given later in this paper) leads to a reduction in the diffusion coefficient, but this does not mean that the advective component is negligible compared to the diffusive one. A ratio smaller than unity, say $D_e/D_{aq} = 0.9$, may very well mean that $D_e^{\mathrm{diffusion}}/D_{aq} = 0.2$ without advection effects. For example, if hydrodynamic dispersion occurs within the channels, then the transition from $D_e/D_{aq} < 1$ to $D_e/D_{aq} \geqslant 1$ is continuous, and there is a region of parameter space for which $D_e/D_{aq} < 1$ is compatible with hydrodynamic dispersion. For example, Ramanan *et al.* [43] estimated the diffusion coefficient of a complex of gadolinium and diethylenetriamine pentaacetic acid (Gd-DTPA) using magnetic resonance imaging with an in-plane resolution of 150 μm × 150 μm. They observed the concentration fields in agar, a highly permeable gel, and in a phototrophic biofilm. The diffusion coefficient in the biofilm was found to be larger than that in the highly permeable gel. Using this comparison, the authors deduced that transport in the biofilm,

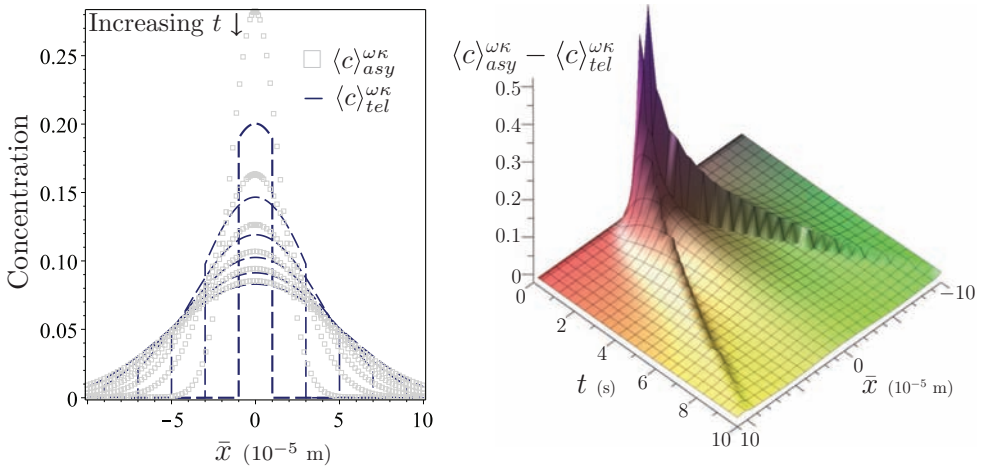

(a) Analytical solutions, $\langle c\rangle^{\omega\kappa}_{asy}$ and $\langle c\rangle^{\omega\kappa}_{tel}$

(b) Difference, $\langle c\rangle^{\omega\kappa}_{asy} - \langle c\rangle^{\omega\kappa}_{tel}$

FIG. 3. (Color online) Illustrations of the telegrapher's and advection-dispersion fundamental solutions for $\langle c\rangle^{\omega\kappa}(\bar{x}, t = 0) = \delta(\bar{x})$, $\partial_t \langle c\rangle^{\omega\kappa}(\bar{x}, t = 0) = 0$, $T = 1$ s, and $D_e = 10^{-10}$ m^2 s^{-1}: (a) Plot of $\langle c\rangle^{\omega\kappa}_{\mathrm{tel}}$ (Telegraph), Eq. (26), and $\langle c\rangle^{\omega\kappa}_{\mathrm{asy}}$ (Gaussian), Eq. (27). Each curve represents the solution at a given time. Notice that the front, in the telegrapher's solution, involves a Dirac distribution. (b) Plot showing how the difference $\langle c\rangle^{\omega\kappa}_{\mathrm{asy}} - \langle c\rangle^{\omega\kappa}_{\mathrm{tel}}$ between the fundamental solutions evolves over time. The telegrapher's equation can be interpreted as an advection-dispersion equation with a wave perturbation that disappears in the long-time limit.

TABLE II. Diffusion coefficients in pure water at 25 °C and corresponding Péclet numbers for example solutes.

Solute	D_{aq} in 10^{-10} m^2 s^{-1}	Ref.	Pe $= \frac{21\times10^{-8}}{D_{aq}}$ from Ref. [2]	Pe $= \frac{7.5\times10^{-10}}{D_{aq}}$ from Ref. [44]
Oxygen	20.0	[19]	$\approx 1.0 \times 10^{+2}$	$\approx 4.0 \times 10^{-1}$
Carbon dioxide	19.2	[19]	$\approx 1.0 \times 10^{+2}$	$\approx 4.0 \times 10^{-1}$
Sucrose	5.2	[19]	$\approx 4.0 \times 10^{+2}$	≈ 1.4
Hexokinase	0.59	[45]	$\approx 3.5 \times 10^{+3}$	$\approx 1.3 \times 10^{+1}$
Linear DNA 10^4 base pairs	8×10^{-4}	[45]	$\approx 2.6 \times 10^{+6}$	$\approx 9.4 \times 10^{+4}$

although they observed $D_e/D_{aq} < 1$, was by both diffusion and advection.

The second part of our argument relies on direct experimental confirmation that the Péclet number within the fluid channels may lie in the range that yields hydrodynamic dispersion effects. Our calculations of the Péclet numbers are based on average velocities, calculated using PIV measurements performed in Refs. [2] and [44]. We remark that these correspond to extra-cluster channels for biofilms grown on flat surfaces and, to the best of our knowledge, experimental data for intracluster velocities or biofilms grown on more complex substrata (e.g., in porous media) do not yet exist. Figure 5 in Ref. [2] supplies an average velocity of $\approx 3 \times 10^{-3}$ m/s for a characteristic length of ≈ 70 μm; and Fig. 5 in Ref. [44] indicates a velocity of $\approx 1.5 \times 10^{-5}$ m/s for a characteristic length of ≈ 50 μm. Using these values, we can calculate the Péclet number associated with the transport of various chemicals for a temperature of 25 °C. The results presented in Table II show that the Péclet number may take large values, especially for macromolecules. The results for large linear DNA macromolecules are presented to illustrate the limit $D_{aq} \to 0$ and to show that a large Péclet number does not necessarily correspond to large hydrodynamic forces. For Pe $\gtrsim$ 1–10, fluctuations in the velocity field within the fluid channels will induce hydrodynamic dispersion effects. We remark that the reference diffusion coefficient should correspond to the solvent in the water channels, rather than pure water, and that D_{aq} in Table II is therefore an upper bound for the reference diffusion coefficients. Consequently, the values of the Péclet numbers presented in Table II should be viewed as lower bounds.

III. MICROSCALE MODELING FORMULATION

As discussed previously, the biofilm can be decomposed into two distinct phases: a cell-EPS matrix phase (ω) and the fluid-channels phase (κ) (see Fig. 2). Within the cell-EPS matrix phase, the solute is transported by diffusion alone but the diffusion coefficient can vary in space. In the channel phase, the solute is transported by diffusion and advection. Delineating explicitly between the bulk water phase and the channels is an important problem that should be carefully addressed in the future. However, for the purposes of this study, we consider an idealized channel phase and suppose that all interfaces are static. This assumption is valid if the time scales associated with the transport phenomena and the growth processes are markedly different (e.g., in Ref. [46]), and can be further justified by the stated aim to understand mass transport itself, rather than its coupling with growth.

By considering conservation of mass for a given solute, the following system of equations can be used to describe transport in this system:

$$\frac{\partial c_\omega}{\partial t} = \nabla \cdot [D_\omega(\mathbf{r}) \nabla c_\omega] \quad \text{in } \mathcal{V}_\omega, \tag{1}$$

$$\mathbf{n}_{\omega\kappa} \cdot [D_\omega(\mathbf{r}) \nabla c_\omega] = \mathbf{n}_{\omega\kappa} \cdot (D_\kappa \nabla c_\kappa) \quad \text{on } \mathcal{A}_{\omega\kappa}, \tag{2}$$

$$c_\omega = c_\kappa \quad \text{on } \mathcal{A}_{\omega\kappa}, \tag{3}$$

$$\frac{\partial c_\kappa}{\partial t} + \nabla \cdot (\mathbf{v}_\kappa c_\kappa) = \nabla \cdot (D_\kappa \nabla c_\kappa) \quad \text{in } \mathcal{V}_\kappa. \tag{4}$$

In these equations, c_α is the pointwise concentration (nutrient or antimicrobial agent) in the phase (α) with ($\alpha = \omega,\kappa$); $D_\omega(\mathbf{r})$, also referred to as D_ω for simplicity, is the diffusion coefficient within the cell-EPS phase (it may vary with spatial position); D_κ is the diffusion coefficient in the channel phase; $\mathcal{V}_\alpha$ is the open bounded set that represents the α phase within the REV; $\mathcal{A}_{\omega\kappa}$ is the interface between the channel phase and the cell-EPS phase; $\mathbf{n}_{\omega\kappa}$ is the unit vector normal to $\mathcal{A}_{\omega\kappa}$ pointing from ω to κ; and $\mathbf{v}_\kappa$ is the velocity field in the fluid phase. We will suppose that the velocity field is known pointwise throughout the entire system, in order to focus on mass, rather than momentum, transport (the reader is referred to Ref. [47] for an extensive discussion on fluid flow in biological media). We will also assume that D_ω *can be actively modified by the microorganisms* but that its average value over a REV varies slowly throughout the biofilm.

For simplicity, *we will only use averaging I in Fig. 2*, with an extension to averaging II that would involve similar models but that requires one to consider the solid and the biofilm–bulk-fluid boundaries. We remark that averaging II will produce macroscale models for the biofilm with reduced dimensionality, i.e., a three-dimensional biofilm will be treated as a two-dimensional (2D) interface. This idea is reminiscent of the notion of an effective boundary condition that was discussed by Veran *et al.* [48] in the case of rough reactive walls. We will explore this idea further in future work. In addition, we emphasize that this distinction only represents a schematic view of the problem and that, from a theoretical point of view, the only relevant criterion is the separation of length scales, i.e., we require $R \ll L$.

In Eq. (2), we have assumed that the velocity field vanishes on $\mathcal{A}_{\omega\kappa}$ so that the interfacial flux across the boundary is purely diffusive. We have further assumed that the system is at thermodynamic equilibrium, and that equality of the chemical potentials on $\mathcal{A}_{\omega\kappa}$ leads to continuity of the concentrations there. In practice, this purely thermodynamic constraint could be easily relaxed by applying a suitable constitutive law for the chemical potentials. For instance, in diluted cases, this equality is often written in terms of a jump condition for the concentrations, $c_\omega = \mathcal{K} c_\kappa$ on $\mathcal{A}_{\omega\kappa}$, in which $\mathcal{K}$ is a function of the pressure and the temperature. For the purposes of the upscaling performed in the remainder of this study, the only constraint that is mandatory is that this relationship between c_ω and c_κ should be affine. For simplicity, we restrict attention to the case $c_\omega = c_\kappa$ on $\mathcal{A}_{\omega\kappa}$, noting that an extension to $c_\omega = \mathcal{K} c_\kappa$

on $\mathcal{A}_{\omega\kappa}$ would be straightforward, using a simple change of variables.

IV. MULTISCALE PERTURBATION ANALYSIS

In this section, the transport equation in each phase is averaged in space (as defined in Fig. 2), and the pointwise fields are decomposed into an averaged part plus a perturbation. The averaged component is allowed to vary on a characteristic length scale R within a macroscopic domain of length L, while the perturbation varies with a characteristic length l_κ, where we assume $L \gg R \gg l_\kappa$ in order to perform an asymptotic analysis.

A. Definitions

First, we define the volume of the phase ($\alpha = \omega,\kappa$), $V_\alpha = \int_{\mathcal{V}_\alpha} dV$, and the total volume of the REV, $V = V_\omega + V_\kappa$. We denote the superficial average of any tensor field π_α (for tensors of order 0, 1, or 2) by $\langle \pi_\alpha \rangle = \frac{1}{V_\alpha} \int_{\mathcal{V}_\alpha} \pi_\alpha \, dV$. We define the volume fraction (which we take to be constant throughout the biofilm) of the α phase, $\varepsilon_\alpha = \frac{V_\alpha}{V}$, and the intrinsic average, $\langle \pi_\alpha \rangle^\alpha = \frac{1}{\varepsilon_\alpha} \langle \pi_\alpha \rangle$. We will also use $\langle \pi \rangle^{\omega\kappa} = \varepsilon_\omega \langle \pi_\omega \rangle^\omega + \varepsilon_\kappa \langle \pi_\kappa \rangle^\kappa$.

We will perform a perturbation analysis by considering decompositions of the form

$$\pi_\alpha = \langle \pi_\alpha \rangle^\alpha + \tilde{\pi}_\alpha. \tag{5}$$

The motivation for this decomposition is that the separation of length scales will impose physical constraints on the perturbation and we will exploit these constraints to make approximations. At this point in the developments, however, it is not possible to determine the validity of these approximations, so that we can only estimate *a posteriori* the domains of validity of the models. Further, these assumptions, such as the separation of length scales, are not intrinsic to a medium, rather they are process dependent. In other words, for the same biofilm, a homogenized model may be valid for a given value of the flow rate but invalid for a larger one. Equally, it may be valid for a given experimental time scale and not for a shorter one.

The volume average definitions stated above are general in form, and may be used in several ways. Determining the most relevant averaging volume is highly problem specific, depending on the properties of the biofilm and the flow, and on the degree of complexity and precision required.

B. Averaged equations

Transport equations (1) and (4) are averaged in space in the following way to obtain a biofilm-scale description of the system. First, integrals of derivatives are expressed as derivatives of integrals plus surface terms by exploiting general transport and spatial averaging theorems [49]. Secondly, we use the decomposition specified by Eq. (5), along with the assumed separation of scales, $l_\kappa \ll R \ll L$, to eliminate nonlocal terms, i.e., integrals that cannot be calculated locally on the representative volume. Some guidelines are given in Appendix A, and detailed descriptions can be found in Refs. [35,50]. In this way, we arrive at the following system of macroscopic equations for $\langle c_\omega \rangle^\omega$ and $\langle c_\kappa \rangle^\kappa$:

$$\begin{aligned}
&\varepsilon_\omega \frac{\partial \langle c_\omega \rangle^\omega}{\partial t} - \left(\frac{1}{V} \int_{\mathcal{A}_{\omega\kappa}} \mathbf{n}_{\omega\kappa} D_\omega \, dA \right) \cdot \nabla \langle c_\omega \rangle^\omega \\
&\quad = \varepsilon_\omega \nabla \cdot \left[\langle D_\omega \rangle^\omega \left(\nabla \langle c_\omega \rangle^\omega + \frac{1}{V_\omega} \int_{\mathcal{A}_{\omega\kappa}} \mathbf{n}_{\omega\kappa} \tilde{c}_\omega \, dA \right) \right] \\
&\qquad + \frac{1}{V} \int_{\mathcal{A}_{\omega\kappa}} \mathbf{n}_{\omega\kappa} \cdot (D_\omega \nabla \tilde{c}_\omega) \, dA + \varepsilon_\omega \nabla \cdot \left\langle \tilde{D}_\omega \nabla \tilde{c}_\omega \right\rangle^\omega ,
\end{aligned} \tag{6}$$

$$\begin{aligned}
&\varepsilon_\kappa \frac{\partial \langle c_\kappa \rangle^\kappa}{\partial t} + \varepsilon_\kappa \langle \mathbf{v}_\kappa \rangle^\kappa \cdot \nabla \langle c_\kappa \rangle^\kappa \\
&\quad = \varepsilon_\kappa \nabla \cdot \left[D_\kappa \left(\nabla \langle c_\kappa \rangle^\kappa + \frac{1}{V_\kappa} \int_{\mathcal{A}_{\omega\kappa}} \mathbf{n}_{\kappa\omega} \tilde{c}_\kappa \, dA \right) \right] \\
&\qquad + \frac{1}{V} \int_{\mathcal{A}_{\omega\kappa}} \mathbf{n}_{\kappa\omega} \cdot (D_\kappa \nabla \tilde{c}_\kappa) \, dA - \varepsilon_\kappa \nabla \cdot \langle \tilde{\mathbf{v}}_\kappa \tilde{c}_\kappa \rangle^\kappa .
\end{aligned} \tag{7}$$

We remark that Eqs. (6) and (7) contain integrals involving correction terms to the average concentrations. To close the problem and obtain a macroscopic formulation for $\langle c_\alpha \rangle^\alpha$ ($\alpha = \omega,\kappa$), it remains to express these correction terms $\tilde{c}_\alpha$ as a function of $\langle c_\alpha \rangle^\alpha$ and its derivatives. This is done in two steps. First, the boundary-value problem governing the perturbations is derived. A careful analysis in terms of linear differential operators and/or Green's functions then yields a suitable closure.

C. Perturbations

Since $\tilde{\pi}_\alpha = \pi_\alpha - \langle \pi_\alpha \rangle^\alpha$, equations for the perturbations can be obtained by subtracting suitable multiples of Eqs. (6) and (7) from Eqs. (1) and (4), respectively. In addition, we may neglect derivatives of averaged quantities because, in the continuum limit, the REV can be treated as a "macroscopic point," i.e., there is a separation of the length scales $R \ll L$ (cf. detailed discussions in Ref. [35]). In the general case, the fluctuations satisfy a transient problem and the homogenized equations contain time convolutions (e.g., in Ref. [51]). Such a formulation is useful for describing short-time phenomena and accounts for time nonlocality. Since these short-time phenomena are not relevant for our biofilm application, we will consider only a steady-state problem for the fluctuations. This hypothesis is standard and is generally referred to as the quasistationarity of the perturbation problem [35].

The result of this procedure can be written, in the phase (ω), as

$$\begin{aligned}
&(\langle \nabla D_\omega \rangle^\omega - \nabla D_\omega) \cdot \nabla \langle c_\omega \rangle^\omega \\
&\quad = \nabla \cdot (D_\omega \nabla \tilde{c}_\omega) - \langle \nabla \cdot (D_\omega \nabla \tilde{c}_\omega) \rangle^\omega \quad \text{in } \mathcal{V}_\omega.
\end{aligned} \tag{8}$$

The boundary conditions are

$$\begin{aligned}
&\mathbf{n}_{\omega\kappa} \cdot (D_\omega \nabla \langle c_\omega \rangle^\omega - D_\kappa \nabla \langle c_\kappa \rangle^\kappa) \\
&\quad = \mathbf{n}_{\omega\kappa} \cdot (D_\kappa \nabla \tilde{c}_\kappa - D_\omega \nabla \tilde{c}_\omega) \quad \text{on } \mathcal{A}_{\omega\kappa}
\end{aligned} \tag{9}$$

and

$$\langle c_\omega \rangle^\omega - \langle c_\kappa \rangle^\kappa = \tilde{c}_\kappa - \tilde{c}_\omega \quad \text{on } \mathcal{A}_{\omega\kappa}. \tag{10}$$

In the phase (κ), we have

$$\begin{aligned}
&\nabla \cdot (\mathbf{v}_\kappa \tilde{c}_\kappa) - \langle \nabla \cdot (\mathbf{v}_\kappa \tilde{c}_\kappa) \rangle^\kappa + \tilde{\mathbf{v}}_\kappa \cdot \nabla \langle c_\kappa \rangle^\kappa \\
&\quad = \nabla \cdot (D_\kappa \nabla \tilde{c}_\kappa) - \langle \nabla \cdot (D_\kappa \nabla \tilde{c}_\kappa) \rangle^\kappa \quad \text{in } \mathcal{V}_\kappa.
\end{aligned} \tag{11}$$

Equations (8)–(11) are coupled to Eqs. (4) and (6) and need to be reformulated to facilitate solution. Our goal is to separate the contributions that act on the microscopic level from those that act on the macroscopic level. The first step is to identify the three different macroscopic source terms in these equations: $\nabla\langle c_\omega\rangle^\omega$, $\nabla\langle c_\kappa\rangle^\kappa$, and $\langle c_\omega\rangle^\omega - \langle c_\kappa\rangle^\kappa$. Since Eqs. (8)–(11) are linear in $\tilde{c}_\alpha$ they can be written as $\mathcal{L}(\tilde{\mathbf{c}}) = \mathcal{S}_\mathcal{V}(\nabla\langle c_\omega\rangle^\omega, \nabla\langle c_\kappa\rangle^\kappa)$, and $\mathcal{B}(\tilde{\mathbf{c}}) = \mathcal{S}_\mathcal{A}(\nabla\langle c_\omega\rangle^\omega, \nabla\langle c_\kappa\rangle^\kappa, \langle c_\omega\rangle^\omega - \langle c_\kappa\rangle^\kappa)$, respectively, in which $\tilde{\mathbf{c}} = (\tilde{c}_\kappa, \tilde{c}_\omega)$. $\mathcal{L}$ is the linear operator defined in the bulk phases, $\mathcal{B}$ is the linear operator representing the boundary conditions, and $\mathcal{S}_\mathcal{V}$,$\mathcal{S}_\mathcal{A}$ are the corresponding source terms. By invoking the superposition principle for this boundary-value problem, the solution can be decomposed into three components, each corresponding to one of the source terms. Again recall that we are interested in the continuum limit $R \ll L$, so that these sources can be considered as constant forcing terms and the solution may be written as

$$\tilde{c}_\alpha = \mathbf{b}_{\alpha\kappa} \cdot \nabla \langle c_\kappa\rangle^\kappa + \mathbf{b}_{\alpha\omega} \cdot \nabla \langle c_\omega\rangle^\omega + s_\alpha \left(\langle c_\omega\rangle^\omega - \langle c_\kappa\rangle^\kappa\right), \tag{12}$$

with $\alpha = \omega$ or κ.

A different analysis, using Green's functions (cf. [52]), yields similar expressions for the perturbations. In this case, the solution is also decomposed into components corresponding to the different source terms. The perturbations are then expressed as integrals of the Green's functions and the source terms, over the spatial variable $\mathbf{x}'$ that fixes the position of the δ. In the continuum limit $R \ll L$, we can extract the sources $\nabla\langle c_\omega\rangle^\omega$, $\nabla\langle c_\kappa\rangle^\kappa$, and $\langle c_\omega\rangle^\omega - \langle c_\kappa\rangle^\kappa$ from the integrals and treat these as constant over the length scale of the REV. Therefore, the mapping variables $\mathbf{b}_{\alpha\beta}$ and s_α can also be interpreted as integrals of the corresponding Green's functions over $\mathbf{x}'$.

Substituting Eq. (12) into Eqs. (8)–(11) and collecting terms involving $\nabla\langle c_\kappa\rangle^\kappa$, $\nabla\langle c_\omega\rangle^\omega$, and $\langle c_\omega\rangle^\omega - \langle c_\kappa\rangle^\kappa$ leads to three boundary-value problems (given in Appendix B) that govern $\mathbf{b}_{\alpha\kappa}$, $\mathbf{b}_{\alpha\omega}$, and s_α. These problems are generally solved over a representative portion of the medium, termed the unit cell, and periodic conditions imposed on the boundary between the unit cell and the rest of the system (note that for averaging II in Fig. 2 boundary conditions for the top and bottom should be defined carefully). The last step of this procedure is to ensure uniqueness of the solution to Eq. (12), and of the mapping fields. To do this, we fix $\langle \mathbf{b}_{\alpha\kappa}\rangle^\alpha = \langle \mathbf{b}_{\alpha\omega}\rangle^\alpha = 0$ and $\langle s_\alpha\rangle^\alpha = 0$ to ensure that $\langle \tilde{c}_\alpha\rangle^\alpha = 0$.

V. CLOSED MACROSCOPIC FORMULATIONS

Now that we have explicit expressions for the perturbations, we return to Eqs. (6) and (7) and obtain a closed form for these macroscopic equations.

A. The two-equation model

Substituting Eq. (12) in Eqs. (6) and (7) leads to

$$\varepsilon_\kappa \frac{\partial\langle c_\kappa\rangle^\kappa}{\partial t} + \varepsilon_\kappa \sum_{\alpha=\omega,\kappa} \nabla\cdot(\mathbf{V}_{\kappa\alpha}\langle c_\alpha\rangle^\alpha) = \varepsilon_\kappa \sum_{\alpha=\omega,\kappa} \nabla\cdot(\mathbf{D}_{\kappa\alpha}\cdot\nabla\langle c_\beta\rangle^\alpha) - h(\langle c_\kappa\rangle^\kappa - \langle c_\omega\rangle^\omega), \tag{13}$$

$$\varepsilon_\omega \frac{\partial\langle c_\omega\rangle^\omega}{\partial t} + \varepsilon_\omega \sum_{\alpha=\omega,\kappa} \nabla\cdot(\mathbf{V}_{\omega\alpha}\langle c_\alpha\rangle^\alpha) = \varepsilon_\omega \sum_{\alpha=\omega,\kappa} \nabla\cdot(\mathbf{D}_{\omega\alpha}\cdot\nabla\langle c_\alpha\rangle^\alpha) - h(\langle c_\omega\rangle^\omega - \langle c_\kappa\rangle^\kappa). \tag{14}$$

In Eq. (14), the effective parameters $\mathbf{V}_{\alpha\beta}$, $\mathbf{D}_{\alpha\beta}$, and h can be expressed explicitly as integrals of the mapping fields over the unit cell. For the velocities, we have

$$\mathbf{V}_{\alpha\beta} = -\frac{1}{V_\alpha}\int_{\mathcal{A}_{\omega\kappa}} \mathbf{n}_\alpha\cdot\{D_\alpha[\nabla\mathbf{b}_{\alpha\beta} + (\delta_{\alpha\omega}-\delta_{\alpha\kappa})s_\alpha\mathbf{I}]\}dA - \frac{1}{V_\alpha}\int_{\mathcal{A}_{\omega\kappa}} \mathbf{n}_\alpha\cdot(D_\alpha\delta_{\alpha\beta})dA + \delta_{\alpha\beta}\langle\mathbf{v}_\alpha\rangle^\alpha. \tag{15}$$

For the dispersion tensors, we obtain

$$\mathbf{D}_{\alpha\beta} = \langle D_\alpha[\delta_{\alpha\beta}\mathbf{I} + \nabla\mathbf{b}_{\alpha\beta} + (\delta_{\alpha\omega}-\delta_{\alpha\kappa})s_\alpha\mathbf{I}]\rangle^\alpha - \delta_{\alpha\beta}\langle\tilde{\mathbf{v}}_\alpha\mathbf{b}_{\alpha\beta}\rangle^\alpha. \tag{16}$$

The mass exchange coefficient is

$$h = -\frac{1}{V}\int_{\mathcal{A}_{\omega\kappa}} \mathbf{n}_{\omega\kappa}\cdot[D_\omega(\mathbf{r})\nabla s_\omega]dA = \frac{1}{V}\int_{\mathcal{A}_{\omega\kappa}} \mathbf{n}_{\kappa\omega}\cdot(D_\kappa\nabla s_\kappa). \tag{17}$$

In these equations, we have used $\delta_{\alpha\beta} = 1$ if $\alpha = \beta$ and $\delta_{\alpha\beta} = 0$ if $\alpha \neq \beta$. Here, we have assumed, for simplicity, that these effective properties are constant through the biofilm, so that Eqs. (13) and (14) can be written in a conservative or nonconservative form.

These upscaling approaches, in which the effective parameters are calculated on a representative portion of the system, are becoming increasingly important given recent advances in imaging techniques such as OCT, CLSM, or x-ray microtomography. Instead of determining only volume fractions, porosities, or densities, we can calculate numerically the effective parameters relevant to a specific application by directly using the images obtained.

Physically, Eqs. (13) and (14) mean that we have a continuous macroscopic transport equation for each phase (dual-continua description), in which mass is exchanged with a characteristic time h^{-1}. Similar models have been used to describe mass transport in highly heterogeneous porous media [53] and heat transfer problems [54]. Equations (13) and (14) can be used to describe a broad range of non-Fickian transport phenomena, for which h^{-1} is large compared to other characteristic time scales associated with transport mechanisms. Such situations may arise when microorganisms actively alter the penetration of the solute or expel it from the cell clusters. We also remark that our model equations are quite general, in that they are not geometry specific, and the phases are arbitrary. For example, upon including the bulk water phase in the definition of the channels and imposing a relevant separation of length scales, our model may be adapted to describe non-Fickian transport phenomena induced by biofilm growth in porous media.

B. Telegrapher's equations

On neglecting higher order spatial derivatives, it is possible to approximate Eqs. (13) and (14) by a variant of the telegrapher's equation. This may be written (see Appendix C for details)

$$\left[\frac{\varepsilon_\kappa\varepsilon_\omega}{h}\frac{\partial^2}{\partial t^2}+\frac{\partial}{\partial t}+\mathbf{V}_e\cdot\nabla-\nabla\cdot(\mathbf{D}^*\cdot\nabla)\right]\langle c\rangle^{\omega\kappa}+\left[\frac{\varepsilon_\kappa\varepsilon_\omega}{h}(\mathbf{V}_{\kappa\kappa}+\mathbf{V}_{\omega\omega})\cdot\frac{\partial}{\partial t}\nabla\right]\langle c\rangle^{\omega\kappa}-\left\{\frac{\varepsilon_\kappa\varepsilon_\omega}{h}\nabla\cdot\left[(\mathbf{D}_{\kappa\kappa}+\mathbf{D}_{\omega\omega})\cdot\frac{\partial}{\partial t}\nabla\right]\right\}\langle c\rangle^{\omega\kappa}=0, \tag{18}$$

where

$$\mathbf{D}^*=\sum_{\alpha=\omega,\kappa}\varepsilon_\alpha(\mathbf{D}_{\alpha\omega}+\mathbf{D}_{\alpha\kappa})-\frac{\varepsilon_\kappa\varepsilon_\omega}{h}[\mathbf{V}_{\omega\omega}\mathbf{V}_{\kappa\kappa}-\mathbf{V}_{\omega\kappa}\mathbf{V}_{\kappa\omega}], \tag{19}$$

$$\mathbf{V}_e=\sum_{\alpha=\omega,\kappa}\varepsilon_\alpha(\mathbf{V}_{\alpha\omega}+\mathbf{V}_{\alpha\kappa})=\varepsilon_\kappa\langle\mathbf{v}_\kappa\rangle^\kappa, \tag{20}$$

and

$$\langle c\rangle^{\omega\kappa}=\varepsilon_\omega\langle c_\omega\rangle^\omega+\varepsilon_\kappa\langle c_\kappa\rangle^\kappa. \tag{21}$$

This form of the telegrapher's equation, Eq. (18), is not standard because it contains mixed time-space derivatives. We can simplify it in the case of an infinite isotropic medium by considering the moving frame $\bar{\mathbf{r}}=\mathbf{r}-\mathbf{V}_e t$ and then neglecting mixed time-space derivatives. We can obtain the classical telegrapher's equation (see Appendix C for details):

$$\frac{\varepsilon_\kappa\varepsilon_\omega}{h}\frac{\partial^2\langle c\rangle^{\omega\kappa}}{\partial t^2}+\frac{\partial\langle c\rangle^{\omega\kappa}}{\partial t}=\nabla_{\bar{\mathbf{r}}}\cdot(\mathbf{D}_e\cdot\nabla_{\bar{\mathbf{r}}}\langle c\rangle^{\omega\kappa}), \tag{22}$$

with

$$\mathbf{D}_e=\sum_{\alpha=\omega,\kappa}\varepsilon_\alpha(\mathbf{D}_{\alpha\omega}+\mathbf{D}_{\alpha\kappa})-\frac{\varepsilon_\kappa\varepsilon_\omega}{h}[(\mathbf{V}_{\omega\omega}-\mathbf{V}_e)(\mathbf{V}_{\kappa\kappa}-\mathbf{V}_e)-\mathbf{V}_{\omega\kappa}\mathbf{V}_{\kappa\omega}]. \tag{23}$$

Equation (22) can be interpreted as a wave equation (∂_{tt} dominated) with a perturbation (∂_t) that disappears at early times, or as a diffusion equation (∂_t dominated) with a wave perturbation (∂_{tt}) that disappears in the long-time limit [55,56]. We remark that the wavelike behavior at early times is physically unrealistic for our application because the assumption of quasistationarity of the perturbation problem is not valid in the short-time limit, when nonlocal effects must be considered.

In the mathematical derivation presented in Appendix C, higher order and mixed space-time derivatives represent a deviation from the classical telegrapher's model. Higher order terms must be eliminated for consistency with the first-order closure on the perturbations, Eq. (12). However, the influence of the mixed space-time derivatives upon the solutions is not straightforward, and the complete form is given by Eq. (18). Such models, containing mixed derivatives, have been discussed previously in Refs. [57–59] in the case of two-phase heat conduction which are also known as dual-phase-lagging heat conduction models, or in Ref. [59] for solute contaminant transport. In addition, it is unclear how the standard and nonstandard telegrapher's equations are related for complex initial and boundary conditions. A further drawback of both telegrapher's models, as compared to Eqs. (13) and (14), is that an additional initial condition for the time derivative of the averaged concentration is required.

Beyond these difficulties, the similarities between the two-equation and telegrapher's models are striking and it is tempting to use a telegrapher's model in a semiheuristic manner to describe non-Fickian solute transport in dual-region media. Future work should therefore focus on understanding the exact mathematical relationship between Eqs. (13), (14), (18), and (22), for different choices of boundary conditions, initial conditions, parameters and geometries; numerical simulations should be compared with experimental results in order to determine the exact effect of the mixed time-space derivatives.

C. Time-asymptotic behavior

For $t\gg\frac{h}{\varepsilon_\kappa\varepsilon_\omega}$, Eqs. (13) and (14) are known, at least in the case of a semi-infinite homogeneous medium, to reduce to a single advection-dispersion equation [60,61]:

$$\frac{\partial\langle c\rangle^{\omega\kappa}}{\partial t}+\mathbf{V}_e\cdot\nabla\langle c\rangle^{\omega\kappa}=\nabla\cdot(\mathbf{D}_e\cdot\nabla\langle c\rangle^{\omega\kappa}), \tag{24}$$

that can also be derived directly from the microscale (see [61]). Heterogeneities or the effects of boundary conditions may trigger a departure from the asymptotic situation, as has been illustrated in Ref. [62]. For the variant of the telegrapher's model, a similar analysis, e.g., in terms of spatial moments, can be used to show that Eq. (18) has an asymptotic behavior that can be described by Eq. (24). This is straightforward in the moving frame, i.e., by considering the asymptotic behavior of Eq. (22), and then switching back to the static frame.

The dispersion tensor, Eq. (19), can be decomposed into three components by substituting the expressions for $\mathbf{D}_{\alpha\beta}$ ($\alpha,\beta=\omega,\kappa$), Eq. (16), into Eq. (23). In this way, we arrive at the following expression for the dispersion tensor (see also [63]):

$$\mathbf{D}_e=\underbrace{\sum_{\alpha,\beta=\omega,\kappa}\varepsilon_\alpha\langle D_\alpha(\delta_{\alpha\beta}\mathbf{I}+\nabla\mathbf{b}_{\alpha\beta})\rangle^\alpha}_{\text{Averaged diffusion coefficients and tortuosity}}\underbrace{-\varepsilon_\kappa\langle\tilde{\mathbf{v}}_\kappa(\mathbf{b}_{\kappa\kappa}+\mathbf{b}_{\kappa\omega})\rangle^\kappa}_{\text{Hydrodynamic dispersion}}\underbrace{-\frac{\varepsilon_\omega\varepsilon_\kappa}{h}[(\mathbf{V}_{\omega\omega}-\mathbf{V}_e)(\mathbf{V}_{\kappa\kappa}-\mathbf{V}_e)-\mathbf{V}_{\omega\kappa}\mathbf{V}_{\kappa\omega}]}_{\text{Multiphase dispersion}}. \tag{25}$$

This expression highlights the notion of effective diffusion that was mentioned in the Introduction of this paper. In addition to terms related to tortuosity and hydrodynamic dispersion, the tensor contains a term specific to the multiphase configuration, which involves $\mathbf{V}_{\alpha\beta}$ ($\alpha,\beta=\omega,\kappa$) given in Eqs. (15). This represents a fundamental difference with the expression for the dispersion given in Ref. [40], where the assumption of local mass equilibrium results in the absence of multiphase dispersion. The influence of the hydrodynamic and multiphase dispersion terms depends on the situation. If

there is marked variation in the mean velocities—for example, if the channels have a clear preferred orientation—then the multiphase dispersion term may significantly contribute to the net dispersion effects. However, if the averaged velocity is small—for example, if the channels have no preferred orientation—then the hydrodynamic dispersion originating from velocity fluctuations within the channels will become dominant. We remark further that the effective diffusion is usually characterized by a second-order tensor and can only be described by a scalar when the biofilm is isotropic.

VI. ANALYTICAL AND NUMERICAL RESULTS

A. Asymptotic behavior of the telegrapher's equation

It is important to realize that, although an advection-dispersion equation such as Eq. (24) may seem more familiar than Eqs. (13) and (14) or Eq. (18), there are a number of aspects that make it less pertinent from a theoretical point of view. One important feature of Eq. (24) is that, unlike Eq. (22), its solutions can propagate with infinite speed. Further, since there is no characteristic time associated with mass exchange in Eq. (24), it is only valid when mass exchange can be neglected at the macroscale. Therefore, it is important to understand how the telegrapher's equations and the asymptotic models are related. This can be illustrated by recalling that a fundamental solution to Eq. (24) for a one-dimensional Cartesian geometry on an infinite domain, with $\langle c\rangle^{\omega\kappa}(\bar{x},t=0)=\delta(\bar{x})$, is given by

$$\langle c\rangle^{\omega\kappa}_{\text{asy}} = \Theta(t)\sqrt{\frac{1}{4\pi D_e t}}e^{-(\bar{x}^2/4D_e t)}, \tag{26}$$

where Θ is the Heaviside step function. Similarly, a fundamental solution to Eq. (22) posed on a one-dimensional Cartesian geometry on an infinite domain, with $\langle c\rangle^{\omega\kappa}(\bar{x},t=0)=\delta(\bar{x})$ and $\partial_t\langle c\rangle^{\omega\kappa}|_{t=0}=0$, is given (e.g., [64]) by

$$\begin{aligned}\langle c\rangle^{\omega\kappa}_{\text{tel}} &= \frac{e^{-(t/2T)}}{2}[\delta(\bar{x}-vt)+\delta(\bar{x}+vt)]\\ &+\frac{e^{-(t/2T)}}{2}\left[\frac{1}{2vT}\left(I_0(\rho)+t\frac{I_1(\rho)}{2T\rho}\right)\Theta(vt-|\bar{x}|)\right],\end{aligned} \tag{27}$$

where $v=\sqrt{\frac{D_e h}{\varepsilon_\omega\varepsilon_\kappa}}$, $T=\frac{\varepsilon_\omega\varepsilon_\kappa}{h}$, $\rho=\frac{\sqrt{v^2t^2-\bar{x}^2}}{2vT}$, and $I_n(\cdot)$ are modified Bessel functions of the first kind.

In Fig. 3(a) we present results showing how these solutions evolve over time, and in Fig. 3(b) we plot their difference, $\langle c\rangle^{\omega\kappa}_{\text{asy}}-\langle c\rangle^{\omega\kappa}_{\text{tel}}$. These figures demonstrate that at long times the telegrapher's equation can be well approximated by the asymptotic model. Standardized moments (especially skewness and kurtosis) can also be used to study the convergence from the two-equation or telegrapher's model towards Eq. (24) (cf. discussions in Ref. [61]).

B. Illustration of the multiphase dispersion effect

To understand further the physical significance of the dispersion terms appearing in Eq. (25), it is helpful to consider the simple axisymmetric configuration of a tube of radius R_1, in which (r,z) represent the radial and axial coordinates (see Fig. 4). The phase (κ) occupies the region $0<r<R_0$

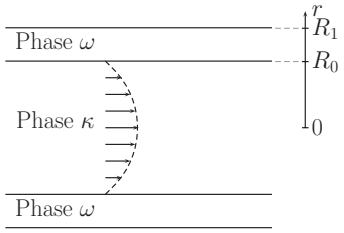

FIG. 4. Schematic diagram depicting the cylindrical geometry of the tube problem.

and the phase (ω) occupies $R_0<r<R_1$. We impose a Poiseuille flow in the phase (κ) described by the velocity $\mathbf{v}=v_0(1-\frac{r^2}{R_0^2})\mathbf{e}_z$, and suppose that $D_\kappa=D_\omega=D$ is constant through space. All components of the dispersion tensor, Eq. (25), corresponding to a concentration surface averaged over the width of the tube, vanish except for its axial component D_e^{zz} which can be written as

$$\begin{aligned}D_e^{zz} &= D-\varepsilon_\kappa\langle[\tilde{\mathbf{v}}_\kappa(\mathbf{b}_{\kappa\kappa}+\mathbf{b}_{\kappa\omega})]^{zz}\rangle^\kappa\\ &+\frac{\varepsilon_\kappa\varepsilon_\omega}{h}\left[\varepsilon_\kappa\varepsilon_\omega\left(V^z_{\kappa\kappa}-V^z_{\omega\omega}\right)^2+V^z_{\omega\kappa}V^z_{\kappa\omega}\right].\end{aligned} \tag{28}$$

A complete solution to this problem is challenging (see, for example, a discussion of a similar problem in Ref. [65]). Here, our goal is to illustrate the different terms that appear in the dispersion tensor rather than to construct an exact solution. We will therefore use simple approximations and dimensional analysis to develop an approximate solution (a rigorous calculation is performed in the next section for a two-dimensional unit cell). As a first step, we will assume that we can approximate hydrodynamic dispersion using Taylor's result

$$-\frac{1}{D}\langle[\tilde{\mathbf{v}}_\kappa(\mathbf{b}_{\kappa\kappa}+\mathbf{b}_{\kappa\omega})]^{zz}\rangle^\kappa\approx\frac{\text{Pe}^2}{48}, \tag{29}$$

with

$$\text{Pe}=\left\langle v_0\left(1-\frac{r^2}{R_0^2}\right)\right\rangle^\kappa\frac{R_0}{D}. \tag{30}$$

In the limit $\varepsilon_\omega\to 0$, this results holds exactly so that we expect it to be a good approximation for ε_ω sufficiently small. In addition, we assume that

$$V^z_{\kappa\kappa}\approx\left\langle v_0\left(1-\frac{r^2}{R_0^2}\right)\right\rangle^\kappa\gg V^z_{\kappa\omega},V^z_{\omega\omega},V^z_{\omega\kappa}. \tag{31}$$

Equation (31) means that we are only considering the physical velocity, and neglect velocity-like terms (such as $V_{\omega\kappa}$ or $V_{\kappa\omega}$) that appear during upscaling, but do not correspond to the average pointwise velocity $\langle v_0(1-\frac{r^2}{R_0^2})\rangle^\kappa$. Using Eq. (31) yields

$$\frac{\varepsilon_\kappa\varepsilon_\omega}{h}\left[\varepsilon_\kappa\varepsilon_\omega\left(V^z_{\kappa\kappa}-V^z_{\omega\omega}\right)^2+V^z_{\omega\kappa}V^z_{\kappa\omega}\right]\approx\frac{\varepsilon_\kappa^2\varepsilon_\omega^2D^2\text{Pe}^2}{hR_0^2}. \tag{32}$$

The dispersion coefficient can then be written as

$$\frac{D_e^{zz}}{D}\approx 1+\text{Pe}^2\left(\frac{\varepsilon_\kappa}{48}+\frac{\varepsilon_\kappa^2\varepsilon_\omega^2D}{hR_0^2}\right). \tag{33}$$

At this point, we need an expression for the exchange coefficient h. This can be determined by computing the closure parameters but is rather tedious. As a simple alternative, we use a dimensional analysis. We know that the exchange coefficient has dimensions (time)$^{-1}$ and corresponds to the inverse of the time it takes for a molecule of solute to visit the entire domain. We will therefore write $h = \frac{AD}{d^2}$, where A is a constant scalar and d is a distance. It yields

$$\frac{D_e^{zz}}{D} \approx 1 + \mathrm{Pe}^2 \left(\underbrace{\frac{\varepsilon_\kappa}{48}}_{\text{Taylor dispersion}} + \underbrace{\frac{\varepsilon_\kappa^2 \varepsilon_\omega^2}{A} \frac{d^2}{R_0^2}}_{\text{Two-phase correction}} \right). \quad (34)$$

We remark that (1) we have $\frac{D_e^{zz}}{D} \geqslant 1$, for all values of Pe, because $D_\kappa = D_\omega = D$ and h does not depend on v_0; (2) the two-phase correction involves the product $\varepsilon_\kappa \varepsilon_\omega$ and therefore disappears in the limit $\varepsilon_\kappa \to 0$ or $\varepsilon_\omega \to 0$; and (3) with these approximations, we still obtain dependence on Pe^2.

From Eq. (34), we see that the multiphase term acts as a correction to the classical hydrodynamic dispersion. Taylor dispersion arises because of the velocity perturbation within the κ phase, while the multiphase term is a consequence of differences between the mean velocities within each phase. This also suggests that the multiphase dispersion term may contribute to net dispersion in cases for which the velocity contrast is relatively large.

C. Longitudinal dispersion in a simple unit cell

In this section, our goal is to illustrate the behavior of the longitudinal component of the dispersion tensor D_e^{xx} in a simple 2D geometry, as described in Fig. 5. To compute D_e^{xx}, we could solve numerically the closure problems presented in Appendix B, and use Eq. (25). However, the dispersion tensor may also be written in a more suitable way for computational purposes (see Davit *et al.* [66] for details):

$$\frac{\mathbf{D}_e}{D_\kappa} = \varepsilon_\kappa [(\mathbf{I} + \langle \nabla \mathbf{B}'_\kappa \rangle^\kappa) - \mathrm{Pe} \langle \mathbf{v}'_\kappa \mathbf{B}'_\kappa \rangle^\kappa] + \varepsilon_\omega [D_\Gamma (\mathbf{I} + \langle \nabla \mathbf{B}'_\omega \rangle^\omega)], \quad (35)$$

where L is a characteristic length, $\mathbf{B}'_\alpha = \frac{\mathbf{B}_\alpha}{L}$, $\mathrm{Pe} = \frac{\sqrt{\langle \mathbf{v}_\kappa \rangle^\kappa \cdot \langle \mathbf{v}_\kappa \rangle^\kappa} L}{D_\kappa}$, $\mathbf{v}'_\kappa = \frac{\mathbf{v}_\kappa}{\sqrt{\langle \mathbf{v}_\kappa \rangle^\kappa \cdot \langle \mathbf{v}_\kappa \rangle^\kappa}}$, and $D_\Gamma = \frac{D_\omega}{D_\kappa}$. $\mathbf{B}'_\alpha$ solves the following

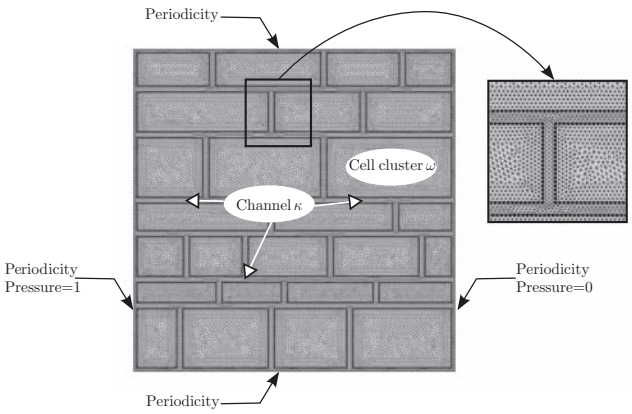

FIG. 5. Illustrations of the unit cell ($\varepsilon_\kappa \approx 0.2$ and $\varepsilon_\omega \approx 0.8$) with the mesh used for computations in COMSOL.

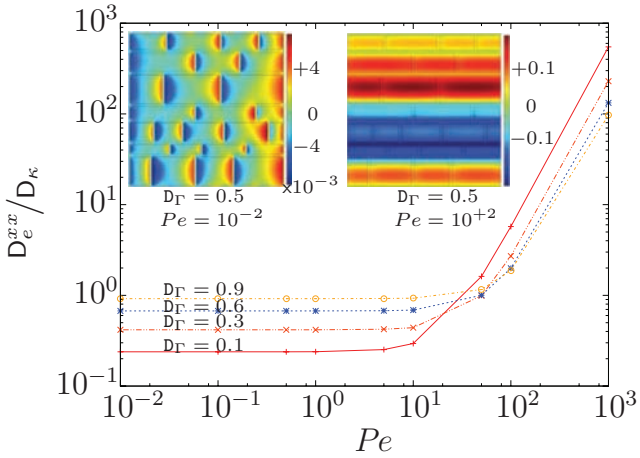

FIG. 6. (Color online) Logarithmic plots of $\frac{D_e^{xx}}{D_\kappa}$ as a function of Pe for different values of D_Γ. Solutions of the closure problem for the x component of $\mathbf{B}'_\omega$ were calculated numerically using COMSOL MULTIPHYSICS 4.2 over the geometry presented in Fig. 5. Scalar $\mathbf{B}'_{\omega,x}$ fields are presented for $D_\Gamma = 0.5, \mathrm{Pe} = 10^{-2}$ (top left) and $D_\Gamma = 0.5$, $\mathrm{Pe} = 10^{+2}$ (top right). This figure shows the complex nonlinear dependence of effective diffusion coefficients upon the system of parameters. For $\mathrm{Pe} \ll 1$, transport is diffusion dominated. For $\mathrm{Pe} \geqslant 10$, hydrodynamic and multiphase dispersion effects become dominant.

boundary-value problem:

$$-\varepsilon_\kappa \langle \mathbf{v}'_\kappa \rangle^\kappa = \nabla \cdot \left(\frac{D_\Gamma}{\mathrm{Pe}} \nabla \mathbf{B}'_\omega \right) \quad \text{in } \mathcal{V}_\omega, \quad (36)$$

$$\nabla \cdot (\mathbf{v}'_\kappa \mathbf{B}'_\kappa) + \tilde{\mathbf{v}}'_\kappa + \varepsilon_\omega \langle \mathbf{v}'_\kappa \rangle^\kappa = \nabla \cdot \left(\frac{1}{\mathrm{Pe}} \nabla \mathbf{B}'_\kappa \right) \quad \text{in } \mathcal{V}_\kappa, \quad (37)$$

with the boundary conditions

$$\mathbf{n}_{\omega\kappa} \cdot \left(\frac{1}{\mathrm{Pe}} \nabla \mathbf{B}'_\kappa - \frac{D_\Gamma}{\mathrm{Pe}} \nabla \mathbf{B}'_\omega \right) = -\mathbf{n}_{\omega\kappa} \left(\frac{1}{\mathrm{Pe}} - \frac{D_\Gamma}{\mathrm{Pe}} \right) \quad \text{on } \mathcal{A}_{\omega\kappa} \quad (38)$$

and

$$0 = \mathbf{B}'_{\kappa\kappa} - \mathbf{B}'_{\omega\kappa} \quad \text{on } \mathcal{A}_{\omega\kappa}. \quad (39)$$

Uniqueness of the solution is obtained by imposing $\varepsilon_\omega \langle \mathbf{B}'_\omega \rangle^\omega + \varepsilon_\kappa \langle \mathbf{B}'_\kappa \rangle^\kappa = 0$.

We used COMSOL MULTIPHYSICS 4.2 (PARDISO solver) to solve this problem and compute the longitudinal coefficient of the dispersion tensor. The computational mesh is presented in Fig. 5, and consisted of triangular meshes (56 570 elements). Solutions were obtained in the following way. First, the velocity and pressure fields were determined by solving the Stokes equations with periodic boundary conditions and a unit pressure difference along the x axis. The resulting velocity field was then used to compute the x component of $\mathbf{B}'_\omega$ (see Fig. 6). This field was used in Eq. (35) to determine $\frac{D_e^{xx}}{D_\kappa}$ for different values of D_Γ and Pe (see Fig. 6). Here, D_e^{xx} is rescaled with D_κ in order to produce results comparable with those of the experimental literature. However, from a theoretical point of view, D_e^{xx} should be rescaled with $(\varepsilon_\kappa + \varepsilon_\omega D_\Gamma) D_\kappa$ in order to eliminate the effect of D_Γ in the limit when $\mathrm{Pe} \to 0$.

Our results highlight the complex, nonlinear dependence of the dispersion tensor upon the system of parameters. For $\mathrm{Pe} \ll 1$, transport is diffusion dominated and only tortuosity affects the longitudinal dispersion coefficient. However, for $\mathrm{Pe} \geqslant 10$, hydrodynamic and multiphase dispersion effects become dominant. These results also show that, even for $\mathrm{Pe} \geqslant 1$, i.e., in the advection-dominated regime, we have a relatively broad range of Péclet numbers for which $\frac{D_e^{xx}}{D_\kappa} \leqslant 1$. *In other words,* $\frac{D_e^{xx}}{D_\kappa} \leqslant 1$ *does not necessarily imply that transport at the microscale is diffusion dominated.*

VII. DISCUSSION

Solute transport in biofilms is often described via a notion of effective diffusion, characterized by the ratio $\frac{D_e}{D_{\mathrm{aq}}}$ of effective, D_e, and reference, $D_{\mathrm{aq}} \approx D_\kappa$, diffusion coefficients. As discussed in the Introduction, the definition of this effective diffusion coefficient, as reported in the literature, is ambiguous. In order to provide a clearer definition and to obtain physical insight, we have used the technique of volume averaging to derive three classes of models for solute transport. One of these models, Eq. (24), is an advection-dispersion equation involving an effective dispersion tensor that can be used to interpret the above notion of effective diffusion. In most cases, this one-equation asymptotic model, Eq. (24), is preferable to the other two formulations, i.e., the two-equation and telegrapher's models. First, it is simple so that it can be easily used to interpret experimental data. Secondly, it has a broad domain of validity, requiring that a time inequality is satisfied, $t \gg \frac{\varepsilon_\kappa \varepsilon_\omega}{h}$, where ε_α is the volume fraction of the phase ($\alpha = \omega, \kappa$) and h is the first-order mass exchange coefficient of the two-equation model (see Sec. V C for more details). To appreciate what constraint this inequality poses, consider passive oxygen diffusion in a biofilm of width $l = 100 - 1000$ μm at temperature 25 °C so that $D = 20 \times 10^{-6}$ cm^2 s^{-1} and suppose that there is a purely diffusive flux at the channel-cluster interface. In this configuration, a good approximation for h^{-1} is the characteristic time for a molecule of solute to diffuse across the entire width of the biofilm, i.e., $\frac{l^2}{D} \approx$ 50–500 ms, in which case the previous constraint, for the validity of the one-equation time-asymptotic model, supplies $t \gg$ 50–500 ms. Therefore, for a (macroscopic) characteristic time of a few seconds or minutes, the constraint is satisfied.

This model also has a straightforward physical interpretation, and each component of the dispersion tensor, Eq. (25), can be explicitly identified. Two types of dispersion effects are important. One arises from velocity fluctuations within the channels. The other is due to differences in the mean velocities of the two phases. The consequence of these terms, on a macroscopic level, is the facilitation of solute transport within the biofilm, potentially leading to situations for which $D_e/D_{\mathrm{aq}} > 1$. Therefore, our analysis provides a solid theoretical basis that can be used to interpret data for which $D_e/D_{\mathrm{aq}} > 1$. In addition, Eq. (25) shows that the effective dispersion tensor depends on the geometry of the channel network. This suggests that parameters describing the geometrical properties of these networks, e.g., their connectivity, may be used in empirical laws for D_e, in addition to parameters such as the cell density or the charge of the EPS. We have also shown that $D_e/D_{\mathrm{aq}} < 1$ does not necessarily correspond to a diffusion-dominated regime, contrary to what was proposed in Ref. [41]. This is also illustrated in Fig. 6, where we observe, in a simple unit cell, that $D_e/D_{\mathrm{aq}} < 1$ for a broad range of values of the Péclet number with $\mathrm{Pe} > 1$ (i.e., in the advection-dominated regime).

Interestingly, and to the best of our knowledge, the effect of the macroscopic advective term $\mathbf{V}_e \cdot \nabla \langle c \rangle^{\omega\kappa}$ has not previously been reported in the literature. One must realize that its effect is extremely difficult to detect, especially in a thin biofilm (typically 100-μm thick). Consider a macroscopic Péclet number defined by $\mathrm{Pe}^M = \frac{V_e L}{D_e}$. We remark that, for a characteristic length L which is sufficiently small, the macroscopic advective term may be systematically neglected. Cases for which the advective term may be important correspond to situations in which the channels are oriented parallel to the boundary. In any case, even if this term is negligible, *this does not mean that the effects of advection can be neglected when calculating the net dispersion tensor*.

Even though the one-equation advection-dispersion model is straightforward and widely applicable, there are some situations for which a two-equation model or a telegrapher's model may be more appropriate. Microorganisms within biofilms are known to actively restrict the penetration of antimicrobial agents within the cell clusters [67–69]. For example, positively charged molecules of antibiotics, such as aminoglycosides, can be bound to negatively charged EPS and have limited permeation properties [67]. More recently, Epstein *et al.* [70] have revealed the extent to which biofilms can limit the penetration of liquids and gas. They measured the contact angle of liquid drops on a *Bacillus subtilis* biofilm and showed that its surface remains nonwetting against up to 80% aqueous solutions of ethanol, surpassing the repellency of Teflon and lotus leaves. Using x-ray computed tomography, they have shown that this biofilm can also be impenetrable to gas. In another study, Váchová *et al.* [71] showed that wild yeast biofilms can develop drug resistance "in which specialized cells jointly execute multiple protection strategies." In particular, their analysis shows that the cells selectively create permeable EPS, while coordinated efflux pumps actively expel toxic substances outside the cell clusters.

These results show that biofilms have the capacity to drastically retard the penetration of antimicrobial agents, and even to actively expel toxic substances. In terms of our modeling approach, this means that the interfacial flux between the channel and cluster phases is modified, for example, by reducing D_ω. As a result, the macroscopic mass exchange coefficient h, between the channels and the cell clusters, can be actively controlled by the microorganisms. If h becomes sufficiently small, the dispersion model discussed previously may cease to be valid for the macroscopic time scale of interest, and the two-equation or telegrapher's models are needed. Figure 7 illustrates this temporal behavior. In addition, because we consider abstract phase geometries, these models can be used to describe solute transport in porous media colonized by biofilms. In such systems, biofilms are known substantially to modify mass transport and can be responsible for anomalous behaviours (e.g., in Ref. [72]). Our models can be adapted readily to describe such situations, in the limiting case where the phase (κ) also represents the bulk water phase within the

porous matrix and there is separation of the relevant length scales.

To determine whether a two-equation, a telegrapher's model, or a variation of the telegrapher's model is better suited to biofilms, additional experimental and numerical data are required. Both classes of models can be used to describe non-Fickian transport; both admit a larger range of solutions than the one-equation advection-dispersion model and will provide more flexibility in inverse optimization approaches. In this work, we have shown that telegrapher's models can be viewed as approximations to the two-equation exchange model. In addition, the telegrapher's equation has had a recent resurgence in numerous scientific fields and may represent a reasonable compromise between the simplicity of the one-equation model and the complexity of the two-equation one. It has been used to describe short-time phenomena in heat transfer [73,74] and in other transport problems [55]. Numerical schemes are available to solve this hyperbolic equation, as well as several analytical solutions (e.g., discussions in Ref. [55]). We believe that the telegrapher's or two-equation models may be good candidates for modeling the transport of antimicrobial agents within biofilms and porous media with biofilms, i.e., to describe situations in which advection cannot be neglected within the fluid channels and the solute has a limited permeation within the cell clusters.

VIII. CONCLUSIONS

To summarize, in this paper:

(1) We have proposed three different, but related, classes of models to describe mass transport within porous biofilms: a two-equation model [see Eq. (14)], telegrapher's models [see Eqs. (18) and (22) and Appendix C], and a one-equation time-asymptotic model [see Eq. (24)]. We have derived these models using the method of volume averaging with closure, have obtained an explicit definition for all the parameters, and have discussed the domain of validity of each model (see illustration in Fig. 7). We have also emphasized that future research should explore, mathematically and experimentally, the relationship between the two-equation and telegrapher's models.

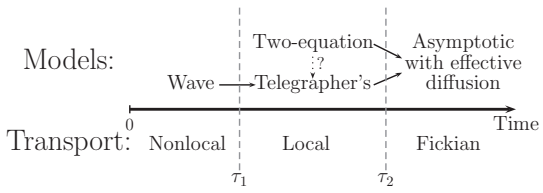

FIG. 7. Illustration of the domains of validity of the different models presented in this paper. τ_1 is a characteristic time associated with the relaxation of the effective parameters and $\tau_2 = \frac{\varepsilon_K \epsilon_\omega}{h}$. For short-time phenomena ($t \ll \tau_1$) transport is nonlocal in time and none of the models presented in this study are suitable. The telegrapher's models exhibit a wave behavior in this regime, but it is a mathematical *artifact* that has no physical significance. For times $\tau_1 \ll t \ll \tau_2$, the transport is non-Fickian and two-equation or telegrapher's models should be used. For $t \gg \tau_2$, the notion of effective diffusion becomes relevant and an advection-dispersion model is sufficient.

(2) We have suggested that the two-equation and telegrapher's models can be used to describe a broad range of non-Fickian transport phenomena that arise in cases where the microorganisms actively limit the penetration of biocides within the cell clusters, and also when biofilms colonize porous media.

(3) We have studied the concept of effective diffusion and have shown that it corresponds to a second-order tensor that appears in the one-equation, time-asymptotic formulation. In the case of porous biofilms, this tensor contains notions of tortuosity, hydrodynamic dispersion, and multiphase dispersion. This result is the main contribution of this study and is consistent with recent results in Ref. [5] that show extremely complex channel networks within porous biofilms. *It also represents a solid theoretical basis for interpreting experimental data for which* $D_e/D_{\text{aq}} > 1$ *and suggests that, even in situations for which* $D_e/D_{\text{aq}} < 1$, *microscale advective transport may contribute to dispersion*.

The primary goal of this paper was to address three questions that were formulated in the Introduction and that can now be answered:

(1) Are hydrodynamic dispersion effects taking place within porous biofilms? *Yes. In Sec. II, we have shown that several different experiments suggest that hydrodynamic dispersion effects do indeed occur within porous biofilm. These experiments can be separated into two classes: measurements of the velocity fields within the channels and determination of the biofilm-scale effective diffusion coefficient. In Sec. II, we have used the velocity fields measured in* Refs. [2] *and* [44] *to show that the* Pe *number can be large enough to produce dispersion effects for several, rather common, chemicals. Further, direct measurements of the effective diffusion coefficients show that the ratio* D_e/D_{aq} *may be larger than unity; an enhanced diffusivity that we hypothesize as being induced by hydrodynamic dispersion effects.*

(2) Can we define an effective diffusion which describes fluid flow within the channels and spatially varying diffusion coefficients within the cell clusters? What are the physical processes corresponding to these effective dispersion coefficients? *Yes. The Fickian effective diffusion model can be used to describe fluid flow within the channels and slowly varying average diffusion coefficients within the cell clusters. We have also shown that the effective diffusion coefficients depend on (1) the topology of the channels' network; (2) the solute's diffusion coefficients in the fluid and the cell clusters; (3) hydrodynamic dispersion effects; and (4) an additional dispersion term intrinsic to the two-phase configuration.*

(3) Should we always use the effective diffusion model to describe solute transport within porous biofilms? What are the alternatives? *No. The Fickian model is only an asymptotic result which has a limited domain of validity. In particular, this model requires a distinct separation of spatial and temporal scales (cf. Figs. 2 and 7). To treat problems where the biofilm is actively restricting the permeation of the solute through the cell clusters (e.g., efflux pumps, surface tension properties), higher order theories such as two-equation or telegrapher's models are more adapted (see Sec. VII). We also emphasize that all these models require a notion of separation of length scales. We have shown that different REVs can be*

used for averaging (see Fig. 2) and that the significance of this constraint may be modified. For instance, averaging I corresponds to a separation of length scales between the REV and the thickness of the biofilm, and averaging II to a separation of length scales between the REV and the width of the biofilm. If such constraints are not satisfied, effective theories cannot be used and the channel and cluster phases should be clearly delineated.

These results have direct implications in terms of modeling solute transport within biofilms; for instance, they show that there are alternatives to the Fickian diffusion model. In addition, we anticipate that this work will stimulate experimental investigations of dispersion effects within porous biofilms by providing a solid theoretical basis for its existence.

Future work will focus on (i) comparing model simulations with experimental data; (ii) calculating effective parameters using images obtained by microscopy techniques; (iii) characterizing the differences between the two-equation and telegrapher's models; (iv) developing effective boundary conditions (averaging II) for relatively thin heterogeneous biofilms; and (v) studying the impact of the reaction rate on the dispersion coefficients for a Damköhler number larger than unity.

ACKNOWLEDGMENTS

This publication was based on work supported in part by Award No. KUK-C1-013-04, made by King Abdullah University of Science and Technology (KAUST). We are also grateful to the two anonymous reviewers for their valuable comments.

APPENDIX A

As previously stated, we will only consider static boundaries. To invert the integral and differential operators, we use the spatial averaging theorems [49]. Upon averaging Eq. (1), we obtain

$$\varepsilon_\omega \frac{\partial \langle c_\omega\rangle^\omega}{\partial t} = \varepsilon_\omega \nabla\cdot\langle D_\omega \nabla c_\omega\rangle^\omega + \frac{1}{V}\int_{\mathcal{A}_{\omega\kappa}} \mathbf{n}_{\omega\kappa}\cdot(D_\omega\nabla c_\omega)\,dA, \tag{A1}$$

where we have exploited the spatial averaging theorem, $\langle\nabla\cdot\boldsymbol{\pi}_\alpha\rangle = \varepsilon_\alpha\nabla\cdot\langle\boldsymbol{\pi}_\alpha\rangle^\alpha + \frac{1}{V}\int_{\mathcal{A}_{\omega\kappa}}\mathbf{n}_{\omega\kappa}\cdot\boldsymbol{\pi}_\alpha\,dA$. Then, in order to separate processes occurring over different length scales, we use the spatial decompositions $D_\omega = \langle D_\omega\rangle^\omega + \tilde{D}_\omega$ and $c_\omega = \langle c_\omega\rangle^\omega + \tilde{c}_\omega$. For example, the first term on the right-hand side reads:

$$\begin{aligned}&\nabla\cdot\langle D_\omega\nabla c_\omega\rangle^\omega\\ &\quad= \nabla\cdot\left[\langle D_\omega\rangle^\omega\left(\nabla\langle c_\omega\rangle^\omega + \frac{1}{V_\omega}\int_{\mathcal{A}_{\omega\kappa}}\mathbf{n}_{\omega\kappa}\tilde{c}_\omega\,dA\right)\right]\\ &\qquad+\nabla\cdot\langle\tilde{D}_\omega\nabla\tilde{c}_\omega\rangle^\omega.\end{aligned} \tag{A2}$$

Other terms, and Eq. (4), are treated similarly. For a detailed description of these procedures, the reader is referred to Ref. [35].

APPENDIX B

The differential equations governing the mapping variables $\mathbf{b}_{\alpha\beta}$ and s_α can be obtained by substituting Eq. (12) into Eqs. (8)–(11). Using the linearity of the differential and boundary operators, we can collect separately terms involving the three different source terms $\langle c_\omega\rangle^\omega - \langle c_\kappa\rangle^\kappa$, $\nabla\langle c_\kappa\rangle^\kappa$, and $\nabla\langle c_\omega\rangle^\omega$. In this way, we arrive at the following set of boundary-value problems:

Boundary-value problem for s_α ($\alpha=\omega,\kappa$), i.e., corresponding to terms involving $\langle c_\omega\rangle^\omega - \langle c_\kappa\rangle^\kappa$:

$$0 = \nabla\cdot(D_\omega\nabla s_\omega) - \varepsilon_\omega^{-1}\langle\nabla\cdot(D_\omega\nabla s_\omega)\rangle \quad \text{in } \mathcal{V}_\omega, \tag{B1}$$

$$0 = \mathbf{n}_{\omega\kappa}\cdot(D_\kappa\nabla s_\kappa - D_\omega\nabla s_\omega) \quad \text{on } \mathcal{A}_{\omega\kappa}, \tag{B2}$$

$$1 = s_\kappa - s_\omega \quad \text{on } \mathcal{A}_{\omega\kappa}, \tag{B3}$$

$$\begin{aligned}&\nabla\cdot(\mathbf{v}_\kappa s_\kappa) - \varepsilon_\kappa^{-1}\langle\nabla\cdot(\mathbf{v}_\kappa s_\kappa)\rangle\\ &\quad= \nabla\cdot(D_\kappa\nabla s_\kappa) - \varepsilon_\kappa^{-1}\langle\nabla\cdot(D_\kappa\nabla s_\kappa)\rangle^\kappa \quad \text{in } \mathcal{V}_\kappa.\end{aligned} \tag{B4}$$

Boundary-value problem for $\mathbf{b}_{\alpha\kappa}$ ($\alpha=\omega,\kappa$), i.e., corresponding to terms involving $\nabla\langle c_\kappa\rangle^\kappa$:

$$\nabla\cdot[D_\omega(\nabla\mathbf{b}_{\omega\kappa} - s_\omega)] = \varepsilon_\omega^{-1}\langle\nabla\cdot[D_\omega(\nabla\mathbf{b}_{\omega\kappa} - s_\omega)]\rangle \quad \text{in } \mathcal{V}_\omega, \tag{B5}$$

$$\begin{aligned}&-\mathbf{n}_{\omega\kappa}D_\kappa = \mathbf{n}_{\omega\kappa}\cdot[D_\kappa(\nabla\mathbf{b}_{\kappa\kappa} - s_\kappa) - D_\omega(\nabla\mathbf{b}_{\omega\kappa} - s_\omega)]\\ &\quad\text{on } \mathcal{A}_{\omega\kappa},\end{aligned} \tag{B6}$$

$$0 = \mathbf{b}_{\kappa\kappa} - \mathbf{b}_{\omega\kappa} \quad \text{on } \mathcal{A}_{\omega\kappa}, \tag{B7}$$

$$\begin{aligned}&\nabla\cdot(\mathbf{v}_\kappa\mathbf{b}_{\kappa\kappa}) - \varepsilon_\kappa^{-1}\langle\nabla\cdot(\mathbf{v}_\kappa\mathbf{b}_{\kappa\kappa})\rangle + \tilde{\mathbf{v}}_\kappa\\ &\quad= \nabla\cdot[D_\kappa(\nabla\mathbf{b}_{\kappa\kappa} - s_\kappa)] - \varepsilon_\kappa^{-1}\langle\nabla\cdot[D_\kappa(\nabla\mathbf{b}_{\kappa\kappa} - s_\kappa)]\rangle^\kappa\\ &\quad\text{in } \mathcal{V}_\kappa.\end{aligned} \tag{B8}$$

Boundary-value problem for $\mathbf{b}_{\alpha\omega}$ ($\alpha=\omega,\kappa$), i.e., corresponding to terms involving $\nabla\langle c_\omega\rangle^\omega$:

$$\begin{aligned}\nabla D_\omega - \langle\nabla D_\omega\rangle^\omega &= \nabla\cdot[D_\omega(\nabla\mathbf{b}_{\omega\omega} + s_\omega)]\\ &\quad - \varepsilon_\omega^{-1}\langle\nabla\cdot[D_\omega(\nabla\mathbf{b}_{\omega\omega} + s_\omega)]\rangle \quad \text{in } \mathcal{V}_\omega,\end{aligned} \tag{B9}$$

$$\begin{aligned}&\mathbf{n}_{\omega\kappa}D_\omega = \mathbf{n}_{\omega\kappa}\cdot[D_\kappa(\nabla\mathbf{b}_{\kappa\omega} + s_\kappa) - D_\omega(\nabla\mathbf{b}_{\omega\omega} + s_\omega)]\\ &\quad\text{on } \mathcal{A}_{\omega\kappa},\end{aligned} \tag{B10}$$

$$0 = \mathbf{b}_{\kappa\omega} - \mathbf{b}_{\omega\omega} \quad \text{on } \mathcal{A}_{\omega\kappa}, \tag{B11}$$

$$\begin{aligned}&\nabla\cdot(\mathbf{v}_\kappa\mathbf{b}_{\kappa\omega}) - \varepsilon_\kappa^{-1}\langle\nabla\cdot(\mathbf{v}_\kappa\mathbf{b}_{\kappa\omega})\rangle\\ &\quad= \nabla\cdot[D_\kappa(\nabla\mathbf{b}_{\kappa\omega} + s_\kappa)] - \varepsilon_\kappa^{-1}\langle\nabla\cdot[D_\kappa(\nabla\mathbf{b}_{\kappa\omega} + s_\kappa)]\rangle^\kappa\\ &\quad\text{in } \mathcal{V}_\kappa.\end{aligned} \tag{B12}$$

These problems are usually solved only on a representative portion of the system using periodic boundary conditions [35].

APPENDIX C

The two-equation model, Eq. (14), can be written using the operator form:

$$\mathcal{L}_{\alpha\omega}\langle c_\omega\rangle^\omega + \mathcal{L}_{\alpha\kappa}\langle c_\kappa\rangle^\kappa = 0 \quad \text{with} \quad \alpha=\omega,\kappa, \tag{C1}$$

where

$$\mathcal{L}_{\alpha\beta} = \delta_{\alpha\beta}\varepsilon_\alpha \frac{\partial}{\partial t} + \varepsilon_\alpha \mathbf{V}_{\alpha\beta}\cdot\nabla - \varepsilon_\alpha \nabla\cdot(\mathbf{D}_{\alpha\beta}\cdot\nabla) + \delta_{\alpha\beta}h - (1-\delta_{\alpha\beta})h. \tag{C2}$$

Given the linearity of these operators, we can write

$$(\mathcal{L}_{\omega\omega}\mathcal{L}_{\kappa\kappa} - \mathcal{L}_{\omega\kappa}\mathcal{L}_{\kappa\omega})\langle c\rangle^{\omega\kappa} = 0. \tag{C3}$$

On neglecting higher order spatial derivatives, it yields

$$\frac{\varepsilon_\kappa\varepsilon_\omega}{h}\frac{\partial^2}{\partial t^2} + \frac{\partial}{\partial t} + \mathbf{V}_e\cdot\nabla - \nabla\cdot(\mathbf{D}^*\cdot\nabla) + \frac{\varepsilon_\kappa\varepsilon_\omega}{h}(\mathbf{V}_{\kappa\kappa}+\mathbf{V}_{\omega\omega})\cdot\frac{\partial}{\partial t}\nabla - \frac{\varepsilon_\kappa\varepsilon_\omega}{h}\nabla\cdot\left[(\mathbf{D}_{\kappa\kappa}+\mathbf{D}_{\omega\omega})\cdot\frac{\partial}{\partial t}\nabla\right] = 0, \tag{C4}$$

where

$$\mathbf{D}^* = \sum_{\alpha=\omega,\kappa}\varepsilon_\alpha(\mathbf{D}_{\alpha\omega}+\mathbf{D}_{\alpha\kappa}) - \frac{\varepsilon_\kappa\varepsilon_\omega}{h}(\mathbf{V}_{\omega\omega}\mathbf{V}_{\kappa\kappa} - \mathbf{V}_{\omega\kappa}\mathbf{V}_{\kappa\omega}), \tag{C5}$$

and

$$\mathbf{V}_e = \sum_{\alpha=\omega,\kappa}\varepsilon_\alpha(\mathbf{V}_{\alpha\omega}+\mathbf{V}_{\alpha\kappa}). \tag{C6}$$

Upon considering an infinite isotropic medium, the moving frame $\bar{\mathbf{r}} = \mathbf{r} - \mathbf{V}_e t$, and the change of variables $(\mathbf{r},t) \to (\bar{\mathbf{r}},\tau)$, we have

$$\frac{\partial}{\partial t} = \frac{\partial}{\partial \tau} - \mathbf{V}_e\cdot\nabla, \tag{C7}$$

and

$$\frac{\partial^2}{\partial t^2} = \left(\frac{\partial}{\partial \tau} - \mathbf{V}_e\cdot\nabla\right)\left(\frac{\partial}{\partial \tau} - \mathbf{V}_e\cdot\nabla\right). \tag{C8}$$

On neglecting the mixed time-space derivatives, we obtain the telegrapher's equation:

$$\left[\frac{\varepsilon_\kappa\varepsilon_\omega}{h}\frac{\partial^2}{\partial\tau^2} + \frac{\partial}{\partial\tau} - \nabla_{\bar{\mathbf{r}}}\cdot(\mathbf{D}_e\cdot\nabla_{\bar{\mathbf{r}}})\right]\langle c\rangle^{\omega\kappa} = 0, \tag{C9}$$

with

$$\mathbf{D}_e = \sum_{\alpha=\omega,\kappa}\varepsilon_\alpha(\mathbf{D}_{\alpha\omega}+\mathbf{D}_{\alpha\kappa}) - \frac{\varepsilon_\kappa\varepsilon_\omega}{h}[(\mathbf{V}_{\omega\omega}-\mathbf{V}_e)(\mathbf{V}_{\kappa\kappa}-\mathbf{V}_e) - \mathbf{V}_{\omega\kappa}\mathbf{V}_{\kappa\omega}]. \tag{C10}$$

Note that neglecting the mixed terms may be done only in the moving frame, so that the model still captures the correct asymptotic behavior.

[1] J. W. Costerton, *The Biofilm Primer—Springer Series on Biofilms* (Springer-Verlag, Berlin, Heidelberg, 2007).
[2] P. Stoodley, D. deBeer, and Z. Lewandowski, Appl. Environ. Microbiol. **60**, 2711 (1994).
[3] A. Massol-Deyá, J. Whallon, and J. Tiedje, Appl. Environ. Microbiol. **61**, 769 (1995).
[4] G. Hildago, A. Burns, E. Herz, A. Hay, P. Houston, U. Wiesner, and L. Lion, Appl. Environ. Microbiol. **75**, 7426 (2009).
[5] M. Wagner, D. Taherzadeh, C. Haisch, and H. Horn, Biotechnol. Bioeng. **107**, 844 (2010).
[6] J. Wimpenny and R. Colasanti, FEMS Microbiol. Lett. **22**, 1 (1997).
[7] J. Wimpenny, W. Manz, and U. Szewzyk, FEMS Microbiol. Rev. **24**, 661 (2000).
[8] M. Van Loosdrecht, C. Picioreanu, and J. J. Heijnen, FEMS Microbiol. Ecol. **24**, 181 (1997).
[9] M. Davey, N. Caiazza, and G. O'Toole, J. Bacteriol. **185**, 1027 (2003).
[10] A. Houry, M. Gohar, J. Deschamps, E. Tischenko, S. Aymerich, A. Gruss, and R. Briandet, Proc. Natl. Acad. Sci. USA **109**, 13088 (2012).
[11] Z. Plalková, EMBO Rep. **5**, 470 (2004).
[12] H. Laue, A. Schenk, H. Li, L. Lambertsen, T. Neu, S. Molin, and M. Ullrich, Microbiology **152**, 2909 (2006).
[13] R. Donlan, Emerg. Infect. Dis. **15**, 881 (2002).
[14] H. Dupin, P. Kitanidis, and P. McCarty, Water Resour. Res. **37**, 2965 (2001).
[15] M. Thullner and P. Baveye, Biotechnol. Bioeng. **99**, 1337 (2008).
[16] G. Kapellos, T. Alexiou, and A. Payatakes, Adv. Water Resour. **30**, 1648 (2007).
[17] B. Goyeau, D. Lhuillier, D. Gobin, and M. Velarde, Int. J. Heat Mass Transf. **46**, 4071 (2003).
[18] P. Stewart, Biotechnol. Bioeng. **59**, 261 (1998).
[19] P. Stewart, J. Bacteriol. **185**, 1485 (2003).
[20] P. Stewart, Biofouling **28**, 187 (2012).
[21] H. Bungay, W. Whalen, and W. Sanders, Biotechnol. Bioeng. **11**, 765 (1969).
[22] J. Matson and W. Characklis, Water Res. **10**, 877 (1976).
[23] D. de Beer, P. Stoodley, F. Roe, and Z. Lewandowski, Biotechnol. Bioeng. **43**, 1131 (1994).
[24] J. Lawrence, G. Wolfaardt, and D. Korber, Appl. Environ. Microbiol. **60**, 1166 (1994).
[25] P. Bishop, T. Zhang, and Y. Fu, Biotechnol. Bioeng. **31**, 143 (1995).
[26] P. Stewart, W. Davison, and J. Steenbergen, Antimicrob. Agents Chemother. **53**, 3505 (2009).
[27] J. McLean, O. Ona, and P. Majors, ISME J. **2**, 121 (2008).
[28] R. Renslow, P. Majors, J. McLean, J. Fredrickson, B. Ahmed, and H. Beyenal, Biotechnol. Bioeng. **106**, 928 (2010).
[29] Y. Davit, G. Iltis, G. Debenest, S. Veran-Tissoires, D. Wildenschild, M. Gerino, and M. Quintard, J. Microsc. **242**, 15 (2010).
[30] G. Iltis, R. Armstrong, D. Jansik, B. Wood, and D. Wildenschild, Water Resour. Res. **47**, W02601 (2011).
[31] L. Fan, R. Leyva-Ramos, K. Wisecarver, and B. Zehner, Biotechnol. Bioeng. **35**, 279 (1990).
[32] R. Hinson and W. Kocher, J. Environ. Eng. **122**, 1023 (1996).
[33] L. Melo, Water Sci. Technol. **52**, 77 (2005).

[34] E. Werner, F. Roe, A. Bugnicourt, M. Franklin, A. Heydorn, S. Molin, B. Pitts, and P. Stewart, Appl. Environ. Microbiol. **70**, 6188 (2004).

[35] S. Whitaker, *The Method of Volume Averaging* (Kluwer Academic Publishers, Dordrecht, 1999).

[36] Y. Davit, G. Debenest, B. D. Wood, and M. Quintard, Adv. Water Resour. **33**, 1075 (2010).

[37] B. Dykaar and P. Kitanidis, Water Resour. Res. **32**, 307 (1996).

[38] P. Stewart and J. Raquepas, Chem. Eng. Sci. **50**, 3099 (1995).

[39] B. Wood and S. Whitaker, Chem. Eng. Sci. **53**, 397 (1998).

[40] Y. Aspa, G. Debenest, and M. Quintard, Int. J. Environ. Waste Manage. **7**, 112 (2011).

[41] H. Horn and E. Morgenroth, Chem. Eng. Sci. **61**, 1347 (2006).

[42] A. Hille, T. Neu, D. Hempel, and H. Horn, Biotechnol. Bioeng. **103**, 1202 (2009).

[43] B. Ramanan, W. Holmes, W. Sloan, and V. Phoenix, Appl. Environ. Microbiol. **76**, 4027 (2010).

[44] D. de Beer and P. Stoodley, *"Microbial Biofilms" in The Prokaryotes: An Evolving Electronic Resource for the Microbiological Ccommunity*, 3rd ed. (Springer Verlag, New York, 2000).

[45] J. Bryers and F. Drummond, Biotechnol. Bioeng. **60**, 462 (1998).

[46] O. Wanner, H. Eberl, E. Morgenroth, D. Noguera, C. Picioreanu, B. Rittmann, and M. V. Loosdrecht, *Mathematical Modeling of Biofilms*, IWA Scientific and Technical Report No. 18 (IWA Publishing, 2006).

[47] G. Kapellos, T. Alexiou, and A. Payatakes, Math. Biosci. **225**, 83 (2010).

[48] S. Veran, Y. Aspa, and M. Quintard, Int. J. Heat Mass Transf. **52**, 3712 (2009).

[49] F. Howes and S. Whitaker, Chem. Eng. Sci. **40**, 1387 (1985).

[50] M. Quintard and S. Whitaker, Transp. Porous Media **14**, 179 (1994).

[51] C. Moyne, Adv. Water Resour. **20**, 63 (1997).

[52] B. Wood, Adv. Water Resour. **32**, 723 (2009).

[53] F. Cherblanc, A. Ahmadi, and M. Quintard, Adv. Water Resour. **30**, 1127 (2007).

[54] M. Quintard, M. Kaviany, and S. Whitaker, Adv. Water Resour. **20**, 77 (1997).

[55] G. Weiss, Physica A **311**, 381 (2002).

[56] G. Uffink, A. Elfeki, M. Dekking, J. Bruining, and C. Kraaikamp, Transp. Porous Media **91**, 547 (2012).

[57] L. Wang and X. Wei, Int. J. Heat Mass Transf. **51**, 1751 (2008).

[58] P. Vadasz, Int. J. Heat Mass Transf. **48**, 2822 (2005).

[59] R. Smith, J. Fluid Mech. **105**, 469 (1981).

[60] F. Zanotti and R. Carbonell, Chem. Eng. Sci. **39**, 263 (1984).

[61] Y. Davit, B. Wood, G. Debenest, and M. Quintard, Transp. Porous Media **95**, 213 (2012).

[62] H. Davarzani, M. Marcoux, and M. Quintard, Int. J. Heat Mass Transf. **53**, 1514 (2010).

[63] M. Quintard, F. Cherblanc, and S. Whitaker, Transp. Porous Media **44**, 181 (2001).

[64] P. Hemmer, Physica A **27**, 79 (1961).

[65] R. Aris, Proc. R. Soc. London, Ser. A **252**, 538 (1959).

[66] Y. Davit, M. Quintard, and G. Debenest, Int. J. Heat Mass Transf. **53**, 4985 (2010).

[67] R. Donlan and J. Costerton, Clin. Microbiol. Rev. **15**, 167 (2002).

[68] K. Lewis, Antimicrob. Agents .Chemother. **45**, 999 (2001).

[69] C. Walsh, Nature (London) **406**, 775 (2000).

[70] A. Epstein, B. Pokroy, A. Seminara, and J. Aizenberg, Proc. Natl. Acad. Sci. USA **108**, 995 (2011).

[71] L. Váchová, V. Šťovíček, O. Hlaváček, O. Chernyavskiy, L. Štěpánek, L. Kubínová, and Z. Palková, J. Cell Biol. **194**, 679 (2011).

[72] J. Seymour, J. Gage, S. Codd, and R. Guerlach, Adv. Water Resour. **30**, 1408 (2007).

[73] C. Cattaneo, C. R. Acad. Sci. **247**, 431 (1958).

[74] D. Joseph and L. Preziosi, Rev. Mod. Phys. **61**, 41 (1989).